Index - Final Report

1. Final report

The final report must be prepared in English. Please fill in the following sections of the template.

1.1 Project details

Project title	Large Scale Fuel Cell System Developed for Peak Shaving
Project identification	10679
Name of the programme which has funded the project (ForskVE, ForskNG or ForskEL)	ForskEL
Name and address of the enterprises/institution responsible for the project	DTU Energy, Kemitorvet, bygn. 207, 2800 Kgs. Lyngby
CVR (central business register)	DK 30 06 09 46
Date for submission	12 of July 2016

1.2 Executive summary

The purpose of the project was to develop:

- High efficiency FC technology based on pressurized HTPEM with high efficiency (>60%, based on Gibbs free energy), long lifetime (20.000 hours) and suitable for large stack modules (>10kW), which can be combined to larger systems (>100kW) for SMART grid and CHP applications.
- An air enrichment strategy for higher cathode performance utilizing waste oxygen from the electrolyzer.
- Understanding of novel solution for safe H_2 and O_2 storage. This is based on a new technique for storage of H_2 and O_2 in supercritical CO_2.
- Simple and effective solution for separation of H_2 from CO_2 by using tailored membrane technology.

FC and MEA optimizations

The effect of utilizing an air enrichment strategy combined with a reduction in temperature to increase durability and maintain performance was examined. Before the project start it was believed that this was a feasible strategy, but data produced during the project showed that a reduction in temperature with oxygen enriched air actually resulted in a significant performance reduction. See figure below:

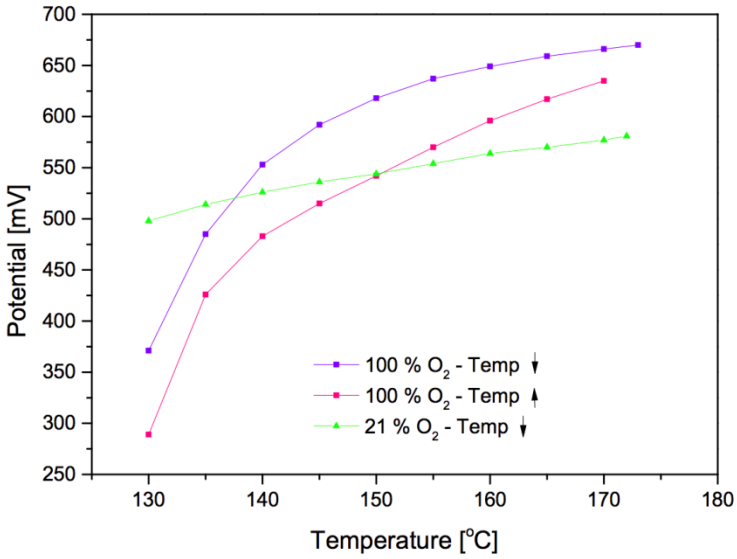

Figure 1: Potential changes during heating (↑), and cooling (↓) for 100% O_2 and air. The current was constant at 200 mA/cm^2 and the flows were set to yield stoichiometries at that current of 2 and 4 for H_2 and O_2, respectively.

This effect has not been observed before and a large part of the project was devoted to understanding why this happened.

The main conclusion of the experimental data were that only a smaller change in temperature was possible from 160 –> 150C, which combined with a small amount of air enrichment could lead to performance gains, as shown in the figure below:

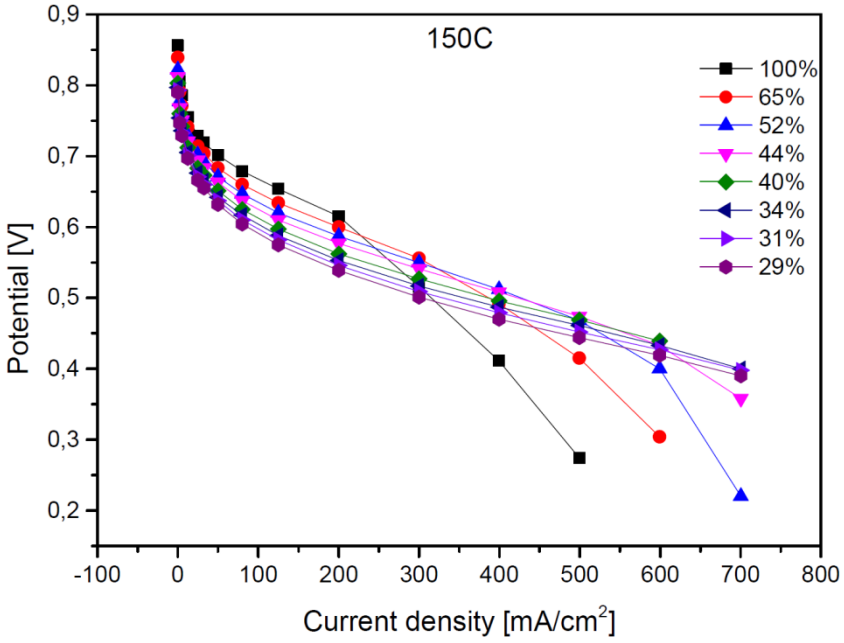

Figure 2: Polarization curves at 150C obtained using conditions simulated enriched strategies with the assumption that pure oxygen and hydrogen is produced and consume from an electrolyzer. Measured at ambient pressure and constant flows throughout the measured current density for each individually polarization curve.

The work on a flexible manufacturing layout for large size MEA's has proven very successful, meaning that issues related to having a flexible manufacturing method for large MEAs (>180 cm^2) and handling of materials have been solved. This is highly important as three external

companies have expressed interest for large MEA's (>600 cm^2) for +20 kW stack modules, and DPS will now be able to manufacture such MEAs.

Recent durability tests at DPS and collaborating partners have demonstrated that the optimized DPS MEAs have a projected lifetime of >20.000 h at 300 mA/cm^2 and 160 °C. The combined results at DTU and DPS means that the project objectives related to the durability of HTPEM fuel cells have been completed.

The concept of the LSD project has successfully been used as basis for an EU project (CISTEM, Construction of Improved HT-PEM MEAs and Stacks for Long Term Stable Modular CHP Units, FCH-JU-2012-1 project no. 325262). Furthermore, this activity is now continued in an application for demonstration of medium sized CHP systems based on HTPEM fuel cells from DPS (four 20 kW CHP systems based on HTPEM is to be demonstrated as part of an application for the current H2020 call (FCH-02-8-2016: Large scale demonstration of commercial fuel cells in the power range of 20-100kW in different market applications).

Hydrogen storage concept

In order to store H_2 produced by electrolysis a new storage concept has been investigated. The concept uses a mixture H_2 and CO_2 in order to increase storage capacity, and reduce the risk associated with storage of H_2. The separation of H_2 and CO_2 is then done using pressure swing where the CO_2 is recycled. Furthermore manufacturing of hollow fiber modules has been investigated, for use as separators.

This report describes a hydrogen storage concept in which an inert buffer gas (CO_2) is used to increase the system safety and therefore increase its acceptance in more locations. If hydrogen is stored in 40:60 molar proportions with CO_2 eventual leaked gas would be flammable, but not explosive. It is a requirement to have the mixture in the gas phase to avoid separation; this is achieved by keeping the temperature above 8 degrees Celsius and the pressure at 100 bars. A system with a total storage volume of 22 m^3 loaded with 124 kg of hydrogen is able to deliver 60.5 Nm^3 H_2/hour for 24 hours to a fuel cell – enough to create 100 kW of electrical power and 66 kW of heat. Some of this power must be used to separate the H_2 from CO_2 before the fuel cell in order to reach a hydrogen concentration of at least 90 %. The CO_2 is recycled to the storage tank and is never released. To achieve the separation goal two separation technologies were considered. A pressure swing model would require 12kWh of the 100kWh output capacity. Alternatively, separation based on commercially available membranes were conceptually shown to be a viable alternative with the potential to improve running efficiency (9 kW power draw) and have lower procurement cost. The total cost for the pressure swing concept (storage and separation) is estimated at 2.4 million DKK, about half of which is attributed to the high pressure storage tanks.

Hydrogen and CO_2 separation

The feasibility of using Hollow Fiber Carbon Membranes for the separation of H_2 and CO_2 was investigated. Cellulose acetate hollow fibers were prepared at NTNU in Trondheim (Norway) and they were subsequently deacetylated and pyrolyzed at SDU. Lab-scale Hollow Fiber modules were constructed using the carbon fibers resulting from the pyrolysis of cellulose hollow fibers at the conditions described in Table 1.

Table 1: Applied pyrolysis conditions.

Sample number	1	2	3	4	5	6	7	8	9
Max Temperature [°C]	550			600			700		
HCl in pyrolysis gas (Ar)	0 %	5 %	10%	0 %	5 %	10%	0 %	5 %	10%

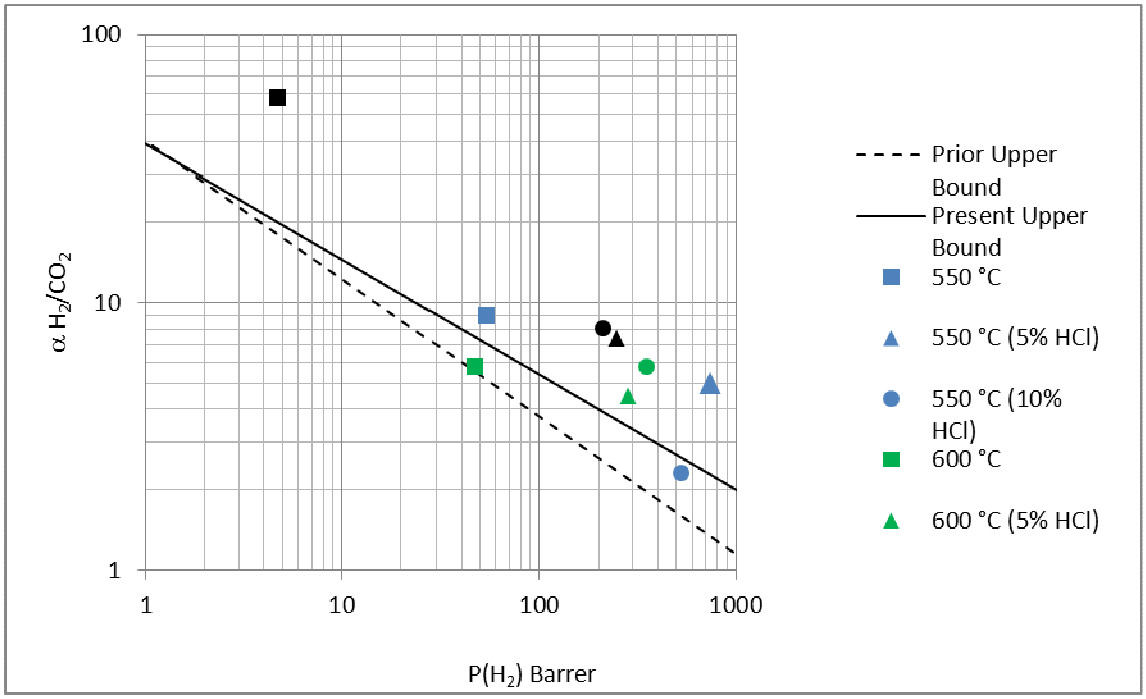

Figure 3 shows the measured permeabilities and selectivities for the constructed modules along with the prior and present Robeson upper bounds, which indicate the state of the art for membrane separation of H_2 and CO_2 as investigated by Robeson et al. in 1999 and 2008.

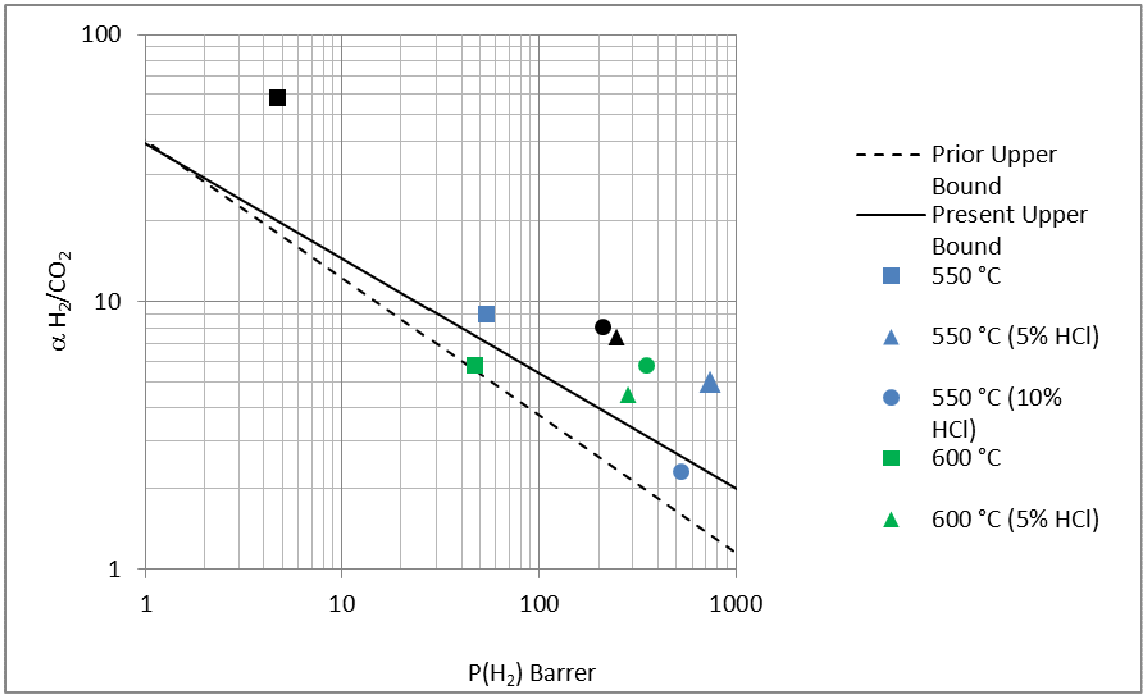

Figure 3. Measured H_2/CO_2-performance and Robeson upper bounds.

The membranes prepared at 550 °C with 5 % HCl in the pyrolysis gas were the most promising, though the required membrane area for purifying a feed stream with a flow rate of 60 STP m^3/h is still hundreds of square meters. The permeance, however, can be improved by manufacturing membranes with a lower wall thickness, reducing the required membrane area. Initial mixed gas measurements confirm that the constructed modules are able to separate H_2 and CO_2, albeit with a lower selectivity than predicted based on pure gases.

Adding HCl to the pyrolysis gas improved the mechanical properties and the permeabilities of the hollow carbon fibers. In most cases the improvement in permeability was accompanied by a decrease in selectivity, which was to be expected.

In summary, the goal of constructing lab scale hollow fiber carbon membrane modules for separation of H_2 and CO_2 was reached and the effects of adding HCl to the pyrolysis gas were documented. However, the process is not yet optimized and needs improvement in order to reduce the required membrane area for the desired separation.

1.3 Project results

1.3.1 WP1 – Fuel & Air/O_2 optimization (Lead: DTU)

Performance evaluations were carried out using different batches of MEAs, supplied by Danish Power Systems [3]. If nothing else is mentioned, the used MEAs had anode Pt loadings of 0.35 mg Pt/cm^2 and cathode platinumloadings of 0.83 mg Pt/cm^2.To examine the Pt loading influence on single cell performance, polarization curves where obtained, but instead of using MEAs with 0.35 mg Pt/cm2 and 0.83mg Pt/cm2 on the anode and cathode, respectively, the Pt loadings were either 0.35 mg Pt/c2 or 1.67 mg Pt/cm2 on both electrodes respectively.

Experiments

The experiments at ambient pressure are divided into two. In the first part, the limited availability of O2 from electrolysis has been taken into consideration. In these experiments it was assumed that a hydrogen stoichiometry of 1.2 is supplied to a fuel cell from a hydrogen storage produced from electrolysis. A corresponding oxygen tank was supplying the fuel cell cathode. In other words, if pure oxygen was used, the maximum oxygen stoichiometry was also 1.2. Higher stoichiometries was obtained by mixing the available amount of oxygen with air. Note that small increments in oxygen stoichiometries will results in large decreases in oxygen concentrations due to nitrogen dilution from added air, e.g. increasing the oxygen stoichiometry from 1.2 to 1.4 will lower the oxygen concentration from 100% to 65%. The fuel cell performance was tested at 140, 150 and 160^{0}C in two series by the polarization curve recording procedure already described. The following conditions were used:

1. All flows were constant throughout the current density region. The H_2 flow was 112 ml/min, corresponding to a stoichiometry of 1.2 at 500 mA/cm2. The O_2 ow was also 112 ml/min, corresponding to a stoichiometry of 1.2 at 1000 mA/cm2. For each temperature 8 additional polarization curves were obtained by mixing synthetic air into the oxygen steam to obtain higher stoichiometries/decreased oxygen concentrations.
2. In the current density range of 0-200mA/cm^2 the flows were kept constant due to lower limit range of the mass flow controllers. Above 200 mA/cm^2 the flows were adjusted to match each specific current set point. The hydrogen stoichiometry was 1.2 for all cases while multiple curves were obtained at different oxygen stoichiometries ((ʌ O2 = 1.2) plus additional synthetic air).

In the second part, the availability of oxygen has not been considered. This means that the purpose of these experiments, is solely to investigate the impact of operating with different oxygen concentration upon fuel cell performance, at different operating temperatures, reactant flows and Pt loading. In order to evaluate the temperature effect on oxygen gain, polarization curves were recorded at temperatures between 120-160^{0}C. For each temperature, the oxygen partial pressure increased in consecutive series. When increasing oxygen partial pressure, MEAs were left for 10 minutes at 200 mA/cm^2 to ensure steady state before re-

cording new polarization curves. To further analyze the oxygen concentration effect, galvanostatic experiments at fixed temperatures, and oxygen and hydrogen stoichiometric flow rates of 4 and 2, respectively but adjusted nitrogen flow, were conducted.

For evaluating the effect from pressurized mode similar polarization curves have been recorded. But, instead of changing the oxygen concentration, the operating pressure was increased. The pressure was increased in increments of 1 bar and the MEA was left for at least 20 min to allow the pressure to stabilize and the fuel cell performance to reach steady state. Experiments have been conducted either with air or pure O_2 as oxidant, and H_2 as fuel. Besides a single experiment, where only the anode side was pressurized, all experiments had equal pressures on both sides.

Results

Constant flow experiments

First we will look at measurements performed at atmospheric pressure with different mixtures of air and oxygen. The idea was here to use all the hydrogen and oxygen produced by electrolysis in the fuel cell. Ideally hydrogen and oxygen is produced and later consumed in equal amounts via electrolysis and fuel cell processes. However, it is well-known that due to the slow oxygen reduction reaction kinetics, a larger oxidant stoichiometry supply is needed for the cathode. Additionally, high flow rates are required to remove the reaction product: water that otherwise could block active sites and inhibit further reaction. To obtain reasonable cathodic stoichiometries and flow rates, while restricted to the available amount of oxygen from electrolysis, it could be necessary to mix the stored oxygen with air. This will result in higher stoichiometries (i.e. higher $\lambda(O_2)$) and flow rates but decreased oxygen concentration.

Consequently, this part of the oxygen enrichment experiments shows how the fuel cell performance is affected if only a limited amount of pure oxygen is available and thus mixed with different amounts of air. The polarization curves recorded using constant flows are presented in Figure 4. All in all, it applies to every of the tested temperatures 140°C, 150°C, 160◦C, that at low current densities, where only a limited amount of the available O_2 is participating in the electro-chemical reaction, the higher the oxygen concentration the better performance. In other words, at low current densities, and constant flows, the performance seems to only depend on the O_2 concentration. However, paradoxically from these results it also becomes clear that at current densities above 200 mA/cm2, increasing amounts of oxygen will lower the performance compared with air. This effect is most pronounced at 140°C but is also found at 160°C,.

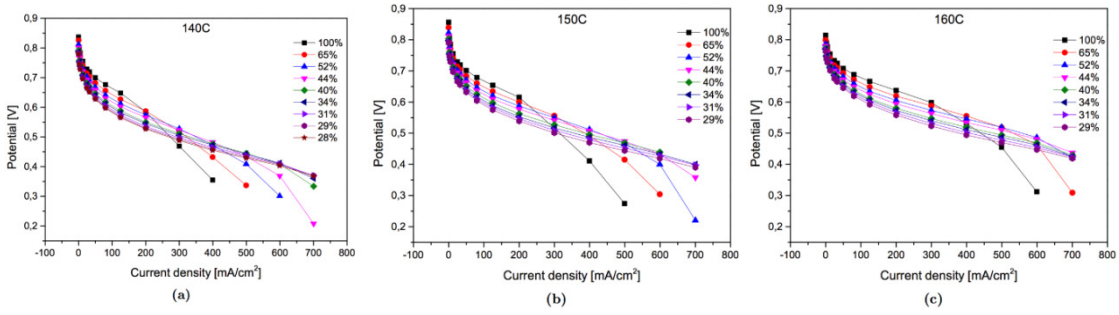

Figure 4: Polarization curves at 140◦C (a), 150◦C (b) and 160◦C (c) obtained with constant flows. □(O_2) at 1 A/cm²: 1.2(100%O_2), 1.4(65%O_2), 1.6(52%O_2), 1.8(44%O_2), 2.0(40%O_2), 2.5(34%O_2), 3.0(31%O_2), 3.5(29%O_2), 4(28%O_2). □(H_2) at 0.5 A/cm₂ : 1.2.

As seen from Figure 4, the maximum current density is 700mA/cm$_2$. This is restricted by the H_2 flow, which corresponds to 1.2 at 500 mA/cm^2. However O_2 is still available in relatively high amounts.

Stoichiometric flow experiments

To further investigate the behavior respons due to limited availability of oxygen it was chosen to repeat the experiments, but instead of overall high constant flows, the flows should be adjusted for each current increment to keep the O_2 and H_2 stoichiometries constant. The polarization curves recorded using stoichiometric flows are presented in Figure 5.

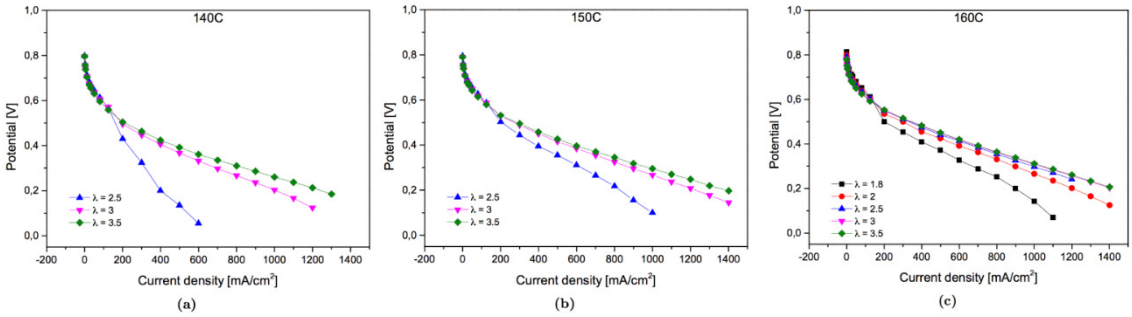

Figure 5: Polarization curves at 140◦C (a), 150◦C (b) and 160◦C (c) obtained with stoichiometric flows.

These results are similar to the results obtained with constant flows, as presented previously; i.e. higher operating temperature requires less mixed-in air. However using stoichiometric flows instead of constant high flows, it is clear that even larger amounts of mixed-in air is required to maintain reasonable performance.

At 140^{0}C and 150^{0}C, oxygen stoichiometries of at least 3, or in other words oxygen concentrations of maximum 31%, are needed. At 160^{0}C, the MEA could work with a stoichiometry of at least 2, corresponding to maximum 40% oxygen. The need for more mixed in air when operating with stoichiometric flows compared to high constant flows, is most likely because the same amount of water is produced in both cases, yet the ratio between water and reactant gases is lower with stoichiometric flows. This means that more added air will help remove the produced water. A common observation, independent of operating temperature, is a lack of performance improvement at low current density with increased O_2 concentration, which was visible for the constant flow experiments, previously presented. Not even at 160 ^{0}C, where the polarization curve obtained with $\lambda = 1.8$ yields a O_2 concentration of 44%. A concentration that did give an improvement for the experiments with constant flow.

Temperature effect experiments

It was decided to determine an optimum in O_2 concentration at a reduced operating temperature. The purpose for a decreased operating temperature, was an increased fuel cell lifetime.[5-7] To do the investigations, any considerations about the availability of O_2 was omitted and abundant supply was ensured, i.e. an O_2 stoichiometry of 4.

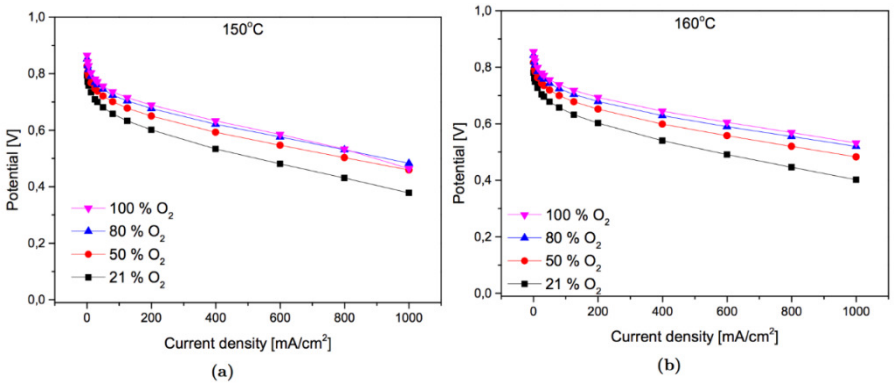

Figure 6: Polarization curves at 150◦C (a), and 160◦C (b) obtained with constant flows.

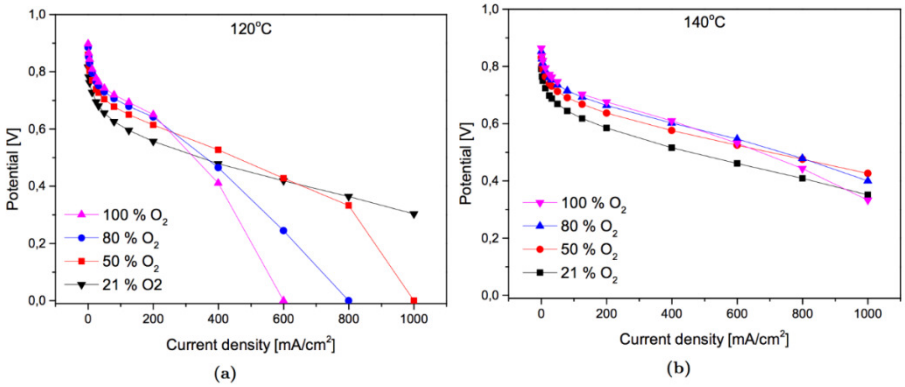

Figure 7: Polarization curves at 120◦C (a) and 140◦C (b) obtained with constant flows.

The results of single cell behavior from experimenting with operating temperature combined with oxygen concentration are represented in Figure 6 and Figure 7. When operating fuel cells at 160^{0}C, an increase in O_2 concentration to 50, 80 or 100% O2 from values corresponding to ambient air, results in improved performance in each of the measured current density points, as seen at Figure 6b. In other words, the best performance is obtained by operating with 100% O_2, whereas diluting the O_2 with N_2 results in reduced performance. This is in agreement with the general accepted idea of using oxygen.

If the operating temperature is reduced to 150^{0}C, as in Figure 6a, the same trend applies for 21, 50 and 80% O2; increased O2 concentration yields improved fuel cell performance in every measured current density point. However, contrary to literature, operating with 100% O_2 introduces some issues at current densities above 800 mA/cm^2, seen by a drop in the 100% O_2 polarization curve below the curve obtained with 80% O_2. Additional reduction in operating temperature to 140^{0}C, seen at Figure 7b, and even further, down to 120^{0}C, seen at Figure 7a, makes this effect even more distinct, as the performances of MEAs operating with pure O_2 tend to exhibit a more and more significant display of performance decay compared to operating with more diluted oxygen flow rates. This means that, as the temperature is reduced, the performances decline at even less pure O_2 flows. Moreover, the decay in performance initiates and becomes much more pronounced at lower current densities at reduced temperatures compared to its higher temperature counterparts. In other words, the worst case scenario is obviously operating at 120^{0}C with 100% O_2. This operating condition, thus yield the lowest potential at 400 mA/cm^2.

To further investigate the temperature effect on fuel cell performance when operating with O_2, galvanostatic measurements were conducted. The potential was recorded at 200 mA/cm^2 and an operating temperature of 170^{0}C. Heating was subsequently turned off and the MEA was allowed to cool. For every 5 ^{0}C temperature reduction, the corresponding po-

tential was recorded. After reaching an operating temperature of 130 ^{0}C, heating was turned on again, and the potential was recorded in 5 ^{0}C temperature increments during heating. For comparison, a similar cooling curve was obtained using 21% O2. The resulting curves are shown at Figure 8.

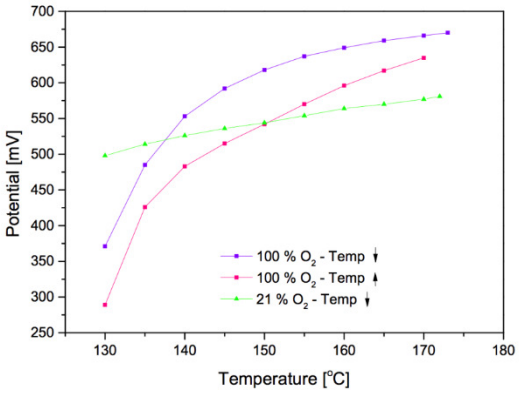

Figure 8: Potential changes during heating (↑), and cooling (↓) for 100% O_2 and air. The current was constant at 200 mA/cm^2 and the flows were set to yield stoichiometries at that current of 2 and 4 for H_2 and O_2, respectively.

During cooling from 170^{0}C to 135^{0}C, while operating with 21% O_2, the potential only decline approx. 50 mV. This reduction in potential appears almost linear, and it is most likely a result of a decrease in proton conductivity. The corresponding curve obtained using 100% O_2 behaves very differently. At high temperatures, the potential is higher compared to the corresponding potential obtained with 21% O_2. However as the temperature is lowered, the potential severely decline. The difference in potential, when operating with 100% O_2 at 170 or 130 ^{0}C is thus approx. 300 mV. The largest potential decline occurred between temperatures of approx. 145 and 130^{0}C. It must, however, be noted that steady state has not been reached before the potential was recorded. This means that, when the temperature reached 130 ^{0}C and heating was yet again turned on, the potential continued to decline until the MEA registered that heating was turned on. This is seen by a difference in potential between the heating and cooling curve obtained with 100% O_2.

From these results, temperatures of 135, and 160^{0}C were singled out. At these temperatures, the potential changes with times were recorded, while the oxygen concentration was switched between 21 and 100 % O_2. The results are presented in Figure 9.

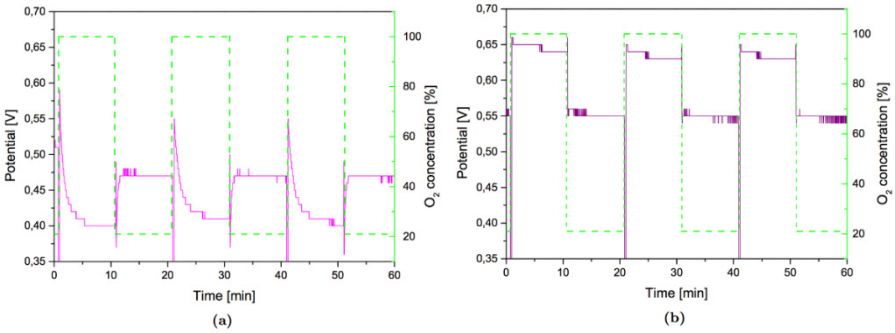

Figure 9: Potential changes (purple line) with time when the O_2 concentration is switched between 21 and 100 %, (green line). The operating temperatures were 135 ◦C (a) and 160 ◦C (b), the current was constant at 200 mA/cm^2 and the flows were set to yield stoichiometries at that current of 2 and 4 for H_2 and O_2, respectively.

At 160^{0}C, seen at Figure 9b, when the O_2 concentration is changed from 21% to 100% O_2 and back again, from 100% to 21% O_2, the potential almost instantaneously changes approx. 90-100 mV. This means that steady state is reached almost right away. However, a huge drop in potential is seen immediately after switching from 21% O_2 to 100%

O_2. This drop is merely due to a sudden dramatic flow reduction, and straight after, the potential increases. Before, a steady potential is reached, a small potential peak (10 mV) is seen, after which the potential appears constant for approx. 5 min, before it again drops approx. 10 mV. It should be noted though, that 10 mV is the smallest load accuracy.

At 135◦C, seen at Figure *9*a, the potential also increases instantaneously to high values when the oxygen concentration is increased, after a rapid potential drop, due to flow conditions similar to the effect seen at 160 ^{0}C. However almost immediately after, the potential starts to gradually decrease. After approx. 5 minutes, it seems that a constant value has been reached. The steady-state potential, when operating with 100% O_2, is thus approx. 75 mV lower than the potential obtained when operating with 21% O_2.

Galvanostatic experiments

To determine at which O_2 concentration, the oxygen gain is negatively affected, it was decided to do galvanostatic measurement at 200 and 800 mA/cm^2 for different temperatures.

The galvanostatic results are presented in Figure 10. These curves clearly indicate the combined temperature and oxygen concentration dependency upon oxygen gain.

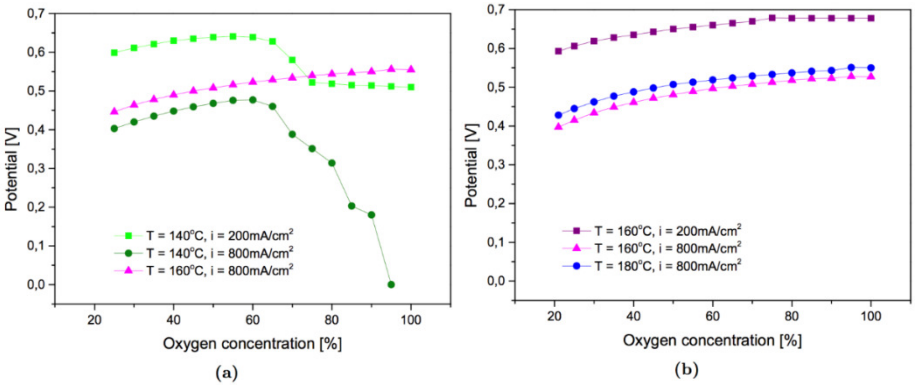

Figure 10: Galvanostatic measurements obtained with N2 flow adjusted in steps of 5 % concentration as desribed in section 4.3.2. (a) shows the potential dependence at 140◦C and 200mA/cm^2 and 140 and 160◦C at 800mA/cm2. (b) shows the potential dependence at 160◦C at 200 and 800 mA/cm^2 and at 180◦C at 800mA/cm2.

At temperatures of 160^{0}C and 180^{0}C, Figure 10b, the fuel cell potential increases with O_2 concentration, independently of the constant current density. This is in agreement with the typical idea of oxygen gain found in literature. Moreover, the temperature increment from 160 to 180◦C increases the potential by approximately 20 mV, possibly owing to increased proton conductivity of the membrane, which was also expected.

However, as also observed from the previous presented polarization curves, reducing the temperature to 140^{0}C, Figure 10a, at first, as the O_2 concentration increases, so does the potential. Yet, when the oxygen concentration is further increased, this introduces a considerably drops in potential. At 140^{0}C, for both current density settings, the potential drop sets in at O_2 concentrations above 60 %. In fact, at O_2 concentrations above 70%, the continuously inclining potential crosses the potential value measured using 21% O_2. Moreover, it can be seen that operating at low current densities (200 mA/cm^2), a minimum potential is reached at O_2 concentrations of 75%. Whereas it seems that the minimum at 800 mA/cm^2 is close to zero potential.

3.5. Platinum loading effect

All previous presented results are obtained using MEAs with Pt loadings of 0.35 and 0.83 mg Pt/cm^2 on the anode and cathode, respectively. If, instead, polarization curves are obtained using MEAs with Pt loadings of 1.67 mgPt/cm^2 on both electrodes, Figure 11b, and these are compared to the previously presented polarization curves, an evident feature emerge. Besides providing a higher potential in every measured current points, operating the fuel cell with 100% O_2 results in improved performance compared to

working with 21% O_2, even if the temperature is reduced to 140^{0}C. In other words, higher Pt loadings seem to improve the fuel cell performance. Most pronounced as an improvement with respect to the previous described performance decay with pure O_2 observed with Pt loadings of 0.35 and 0.83 mg Pt/cm^2 on the anode and cathode, respectively.

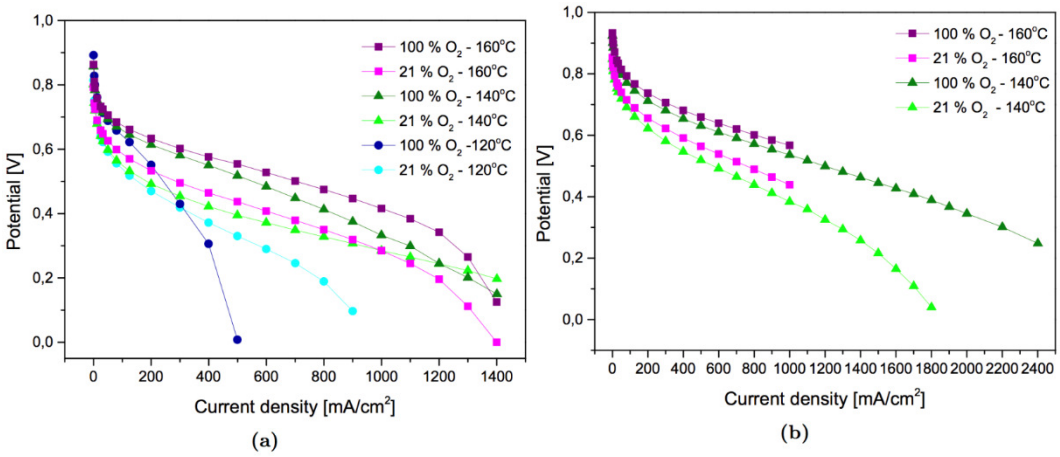

Figure 11: Polarization curves obtained as described in section 4.3.1. The curves in (a) are obtained by use of MEAs with 0.35 mg Pt/cm2 on both electrodes while the Pt loading of the used MEAs in (b) had 1.67 mg Pt/cm^2 on both electrodes. Note: that the x-axis display different ranges.

For comparison, polarization curves using MEAs with Pt loading of 0.35 mg Pt/cm^2 on both electrodes, at 120, 140 and 160^{0}C and oxygen concentrations of 21 and 100% O_2 were also recorded. The resulting curves are presented in Figure 11a. Opposite to the results obtained with high Pt loading, shown at Figure 11b, the polarization curves obtained at low Pt loading are similar to those shown at Figure 6 and Figure 7, which were obtained using 0.35 and 0.83 mg Pt/cm^2 on the anode and cathode, respectively. This means that similar features of reduced performance are visible, working at temperatures of 120 and 140◦C with 100% O_2 compared to the curves obtained by 21% O_2. Furthermore at 160◦C, the performance obtained when working with 100% O_2 is better compared to the polarization curve obtained with 21% O_2.

Pressurization

During the electrolysis process, both H_2 and O_2 can easily be pressurized. This in turn also makes it possible easily to store the gasses under pressure. By doing so, enables the use of the already pressurized gasses as fuel and oxidant in fuel cells, without parasitic energy losses. Operating a fuel cell under pressurized conditions, e.g. reactants, should, according to theory, increase the fuel cell performance.

The experiments presented here are thus conducted in order to investigate the potential gain from operating the fuel cell in a pressurized mode. Due to the fact that H_2 is supplied in an amount with high excess, the hydrogen oxidation reaction requires little overpotential, and the supplied reactant is not diluted by the reaction product (steam), it is believed that the major contributor to increased potential as a result from pressurization may be ascribed to the cathode side. For verification, an experiment where only the anode side is pressurized was conducted. After that, experiments with both anode and cathode pressurized were conducted at various temperatures.

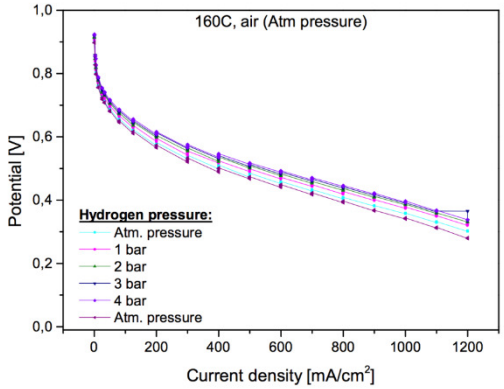

Figure 12: Polarisation curves obtained with different H_2 pressures, at 160◦C using air at atmospheric pressure. Labels indicate gauge pressure.

As seen from Figure 12, increasing the H_2 pressure, results in an increase in potential in all measured current density points. However, the increase in potential is very modest, compared to potentialincreases obtained after pressurizing the cathode as-well. The potential gainat 200 mA/cm^2, attained after increasing the anode (H_2) back-pressure fromambient value to 4 gauge bar (5 bar absolute) is thus 35 mV. A value that remains constant throughout higher current densities. (36 mV at 800 mA/cm^2 and 35 mVat 1200 mA/cm^2.) Another observation is a difference between the two polarization curves with ambient pressure, obtained before and after thepressurized tests. From this it is seen that the "after" result is slightlyworse compared to the initial curve.

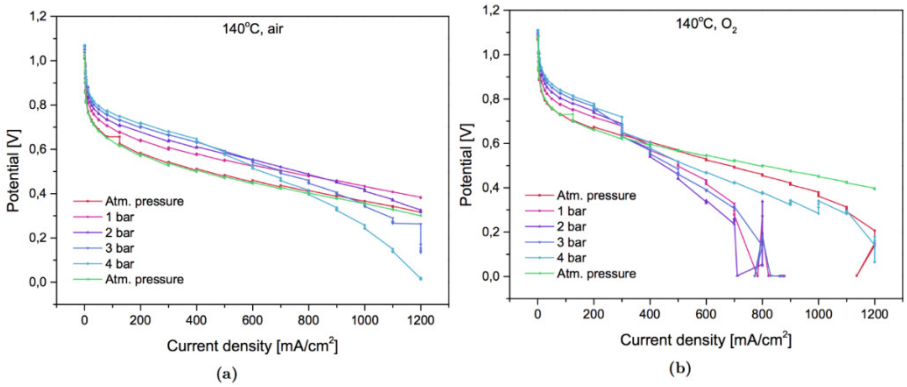

Figure 13: Polarisation curves obtained at 140◦C using either air (a) or O_2 (b) as oxidant. Labels indicate different gauge pressure.

By looking at the results obtained with an operating temperature of 140^{0}C first, Figure 13, it becomes clear that the choice of oxidant has a large influence on the cell behavior when pressurized.

If air is used as oxidant, the initial-, and the final polarization curves obtained at ambient pressure, is almost identical. This is not the case when O_2 is used as oxidant. The two curves obtained at ambient pressure with O_2 as oxidant are nearly identical at low current densities, below approx. 600 mA/cm2. In addition, this cell potential is higher compared to the cell potential attained with air at similar currents, i.e. 566 and 482 mV at 500 mA/cm2 for O_2 and air, respectively.

However, as the current is raised, with O_2 as oxidant, the initial polarization curve clearly suffers from mass transports issues similar to those already observed at 140^{0}C using O_2 at atmospheric pressure as oxidant (see Figure 7b). This means that the cell potential recorded using O_2 instead of air results in a significant reduction at high currents. Returning to ambient pressure, after increments of 1 bar up to the maximum pressure of 4

gauge bar (5 bar absolute), yields a peculiar result. Unexpectedly, the previous observed issues at high currents when O_2 is used as oxidant, is not present now. Meanwhile, increasing the back-pressure 1 bar from ambient pressure, results in a potential gain of approx. 60 mV when air is used as oxidant, Figure 13a. This gain remains more or less constant throughout the measured current densities points. A further pressure increment up to 2, 3, and 4 gauge bar introduces some losses in cell potential at high currents. The potential losses increase with every pressure increment. Hence, when the back-pressure is adjusted to 4 gauge bar, the potential approaches zero V at 1200 mA/cm^2. Meanwhile, at low currents, the cell potential remains highest for the curves recorded with highest pressure.

Similar back-pressure increments from ambient pressure with O_2 used as oxidant yields slightly different results. While, the increased back-pressure result in a potential gain around 50 mV at very low currents (<200mA/cm^2), the potential, however rapidly decreases at higher currents. In fact, the cell potential approaches zero volts at 800 mA/cm^2, after the back-pressure has only been increased 1 bar from ambient conditions. Increasing the pressure further, to 2 and 3 gauge bar, results in similar polarisation curves. Common to the polarization curves obtained with gauge pressures of 1, 2 and 3 bar, are very unstable potentials at high currents. The potentials do fluctuate hundreds of mV. Additionally pressure increment to 4 gauge bar, results in an improved polarization curve compared to the curves obtained at lower pressures. This improved polarization curve approaches the curve obtained at ambient pressure, and thus implies that strong pressurization eliminates the issues present at modest pressures. Returning to ambient pressure further improves the polarization curve as already mentioned.

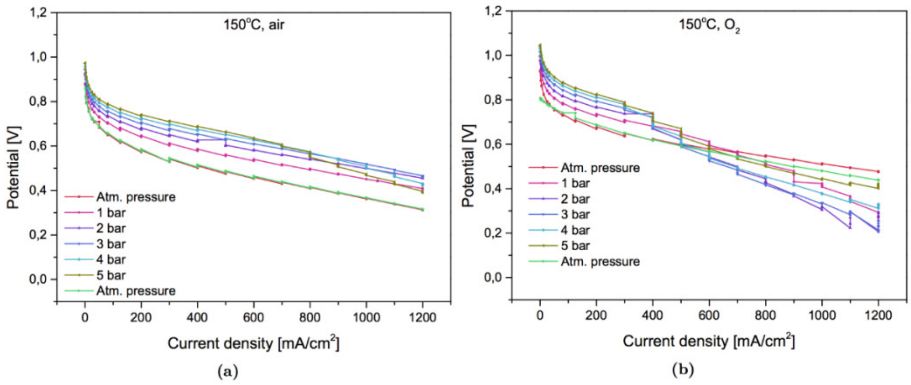

Figure 14: Polarisation curves obtained at 150◦C using either air (a) or O_2 (b) as oxidant. Labels indicate different gauge pressure.

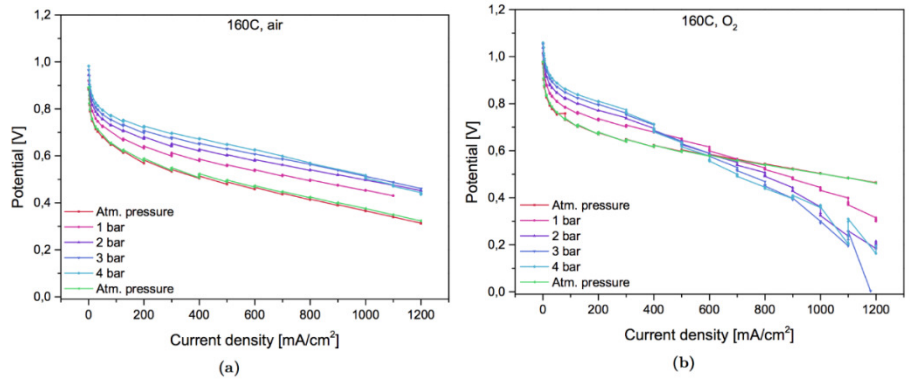

Figure 15: Polarisation curves obtained at 160◦C using either air (a) or O_2 (b) as oxidant. Labels indicate different gauge pressure.

Increasing the temperature 10 ^{0}C to 150^{0}C yields both similar results, but also results that deviate from those obtained at 140 ^{0}C. First of all, the recorded polarization curves

obtained using air as oxidant at 150 ^{0}C at ambient pressure before and after the pressurized curves, Figure 14a, are identical. This is similar to the cell behavior at 140 ^{0}C seen at Figure 13a. If O_2 is used as oxidant instead, the initial and final polarization curves obtained at ambient pressure, are also nearly identical, see Figure 13b, which was not the case at 140 ^{0}C.

Increasing the back-pressure in increments of 1 bar, with air as oxidant, results in improved cell performance throughout the measured current points for 1, 2 and 3 gauge bar, seen by higher cell potentials. It appears that the largest improvement arise when the pressure is changed from ambient pressure to 1 gauge bar. Further pressure increments leads to a continuous smaller potential gain at high current densities. As was seen for pressures above 1 gauge bar at 140^{0}C, potential losses emerge on the polarization curves at high current densities. This also occurs at 150 ^{0}C, at gauge pressures of 4 and 5 bars and very high currents. To a much smaller degree, though.

When O_2 is used as oxidant, Figure 13b, the cell potential increases at low current densities for every pressure increment, as previous observed. Moreover, as was also the case at 140 ^{0}C, when the pressure is increased from ambient value, potential losses emerge at high currents. The potential losses at high current densities increase when the gauge pressure is adjusted to 2 bars. The resulting cell potentials at high currents when the pressure is 3 gauge bar are nearly the same. Yet, when the pressure is increased to 4 and 5 gauge bar, the cell potential at high currents increases with the pressure, as it was seen at 140^{0}C.

Polarization curves obtained after the operating temperature has been further increased to 160 ^{0}C are very similar to those obtained at 150 ^{0}C. With air as oxidant, it appears that the potential losses at high current densities and a pressure of 4 gauge bar is slightly less at 160^{0}C. Otherwise no significant difference between the two operating temperatures are visible when air is used.

Using O_2 as oxidant at an operating temperature of 160 ^{0}C, the resulting polarization curves are again very similar to the corresponding curves obtained at 150 ^{0}C. Yet, the cell potentials are slightly lower at high currents when the pressures are adjusted to 3 and 4 gauge bar. Furthermore, the initial and final polarization curves obtained at ambient pressure and 160^{0}C are more identical, when compared to the corresponding curves at 150^{0}C.

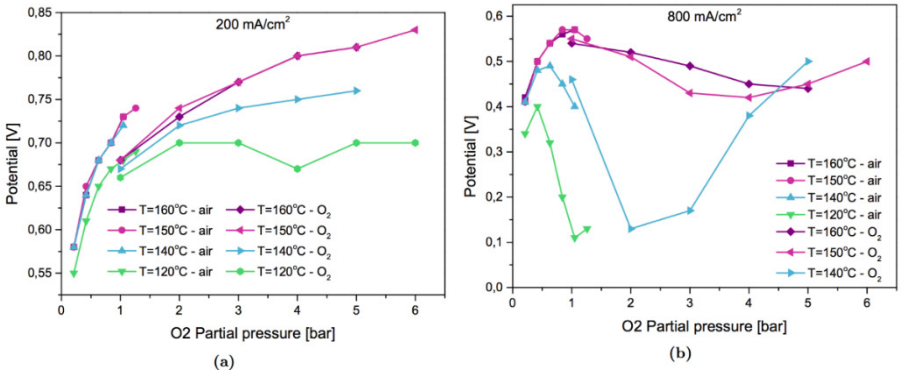

Figure 16: Potential as function of oxygen partial pressure at either 200mA/cm^2 (a) or 800mA/cm2(b). Data is obtained by using either air or pure O_2 in a temperature range of 120-160◦C, as indicated by the legend.

A correlation between O_2 partial pressure, and measured potentials at 200 and 800 mA/cm^2 is shown at Figure 16a and Figure 16b, respectively. The potentials have been extracted from the polarization curves obtained at various operating pressures and different operating temperatures either with air or O_2 as oxidant, as indicated by the graph legend. The pressures were recalculated into O_2 partial pressure to produce the curves in Figure 16. Consequently, the potentials measured using air is correlated to O_2 partial

pressures between 0.21 - 1.26 bar, while the potentials measured using O_2 is referred to O_2 partial pressures between 1 and 6 bar (absolute).
The overall tendency of the measured potentials at 200 mA/cm^2, is that the potentials increases with temperature and O_2 partial pressure. In detail, it becomes clear that the measured potentials using air as oxidant are almost identical in the whole O_2 partial pressure region for temperatures between 140-160 ^{0}C. The corresponding potentials obtained at 120 ^{0}C are on the other hand lower. Moreover, the measured potential at 120^{0}C does not increase as much with operating pressure as the potentials from the other temperatures. This is seen by a larger difference in potential at these temperatures at high pressures compared to the potential difference at low pressures.
Similar results can be observed when O_2 is used as oxidant. However, only the potentials measured at 150 and 160 ^{0}C are alike. At O_2 partial pressures above 2 bar, a clear separation in potentials are measured between the other operating temperatures. In total this means that at 160 ^{0}C, the cell potential increases from 580 to 810 mv when the O_2 partial pressure is increased from 0.21 to 5 bar, which corresponds to a potential gain of 230 mV. At 140^{0}C, the corresponding potential gain is 180 mV, and at 120^{0}C, the gain is reduced to 150 mV.
If we look on the measured potentials at 800 mA/cm^2, Figure 16b, the overall picture is fairly different from that at 200 mA/cm^2. Very small O_2 partial pressure increments above 0.21 bar results in an increase in potential. However relatively rapid the potential reaches a maximum value after which it decreases. The partial pressures where the peak occurs are dependent on operating temperature. At low operating temperatures the potential starts to decrease at smaller O_2 partial pressure compared to the turning point for higher operating temperatures. However, as the O_2 partial pressure is further increased, the potential surprisingly goes through a minimum. Again, it seems temperature dependent at which O_2 partial pressure the minimum occurs.

3.8 A possible explanation of the unexpected results

How can this behavior be explained? First of all, it is important to notice that the paradoxically oxygen phenomena is proportional to the amount of catalyst in the MEA. Compare Figure 7a with Figure 11a. In Figure 11a at 120◦C and 1bar of O_2 and with 0.35 mg Pt/cm^2 the mass transport problem starts at ca. 100 mA/cm^2 whereas in Figure 7a also at 120◦C and 1bar of O_2 but with 0.83 mg Pt/cm^2 it starts at ca. 200 mA/cm^2.This means that the phenomena is due to changes at the three phase boundary of the catalyst and only to a small extent to other factors for example the thickness of the catalyst layer. We also know that phosphoric acid has a tendency to stick to the surface of the platinum in the catalyst [8, 9] and we know from our experiments with CO in the cathode gas [10] that it is possible to move around with the phosphoric acid in the platinum catalyst. Oxygen also has a certain affinity to the platinum surface especially at lower temperatures [11, 12]. If the oxygen pressure is increased, we will expect two things: The activity of O_2 on the cathode will go up and some of the phosphoric acid will be pushed away from the platinum surface and out against the three face boundary. Due to the higher activity of O_2 an increase in potential will be seen at lower current densities, however it is expected that the onset of mass transport problems will start earlier at higher current densities due to a thicker layer of phosphoric acid. If the pressure of O_2 is increased even more the phosphoric acid is pushed further away, out to edge of the platinum particle, now giving a thinner layer of phosphoric acid at the three phase boundary and thus a later onset of the mass transport problems. This is exactly what we see in Figure 16b. A further proof for this model is found by comparing Figure 13a with Figure 13b. It is seen that with compressed air where the increase in oxygen activity is rather small the polarization curve at atmospheric pressure is almost the same before and after the pressurized experiments. In contrast to this in the experiments with compressed oxygen the polarization curve at atmospheric pressure is improved after the experiments with high oxygen pressure

indicating that some the phosphoric acid blocking the three phase boundary has been pushed away.

Conclusions

It has been shown that increasing the oxygen pressure instead of increasing the cell potential at higher current densities and low temperatures in a HT-PEM fuel cell decreases the potential and at even higher pressures again increase the potential. In this connection the presence of nitrogen seems of little importance. A possible explanation of this peculiar behavior is a competition between oxygen and phosphoric acid on the surface of the platinum particles in the catalyst on the cathode side. An increasing pressure of oxygen will push phosphoric acid away from the main part of the platinum particle and out against the three phase region and in this way increasing the onset of the mass transport problems. At even higher oxygen pressure the amount of phosphoric acid will also be reduced at the three phase boundary again moving the transport problems to higher current densities. This behavior will probably be found to a smaller or larger degree in all HT-PEM fuel cells, but not in LT-PEM fuel cells, since the acid here is bound to the membrane.

Ways to reduce the problem could be 1) to change the surface of the platinum by alloying it with another metal 2) changes the size of the platinum particles, smaller particles are expected to keep less phosphoric acid at the edges 3) changes or make additions to the support material for the platinum particles so that it will concentrate less phosphoric acid at the three phase boundaries.

1.3.2 WP2 – Electrode and membrane optimisation (Lead: DTU)

The objectives of this WP was to investigate how to meet the project objectives by:

- Reduced platinum loading
- Membrane optimization
- Cell optimization

The two last aspects have been thoroughly investigated and the results are shown in WP3.

The reduction in platinum loading was thought possible due to the oxygen enrichment of the cathode air. While oxygen enrichment does provide an additional 60-90 mV in performance (and thus higher electrical efficiency of the fuel cell) it proved unfeasible to just reduce the catalyst loading on the cathode. Such a change would require substantial optimization of the cathode catalyst layer as the properties and performance is governed by the acid redistribution interacting with the thickness / porosity of the layer. Thus, a reduced platinum loading would require an optimization beyond the scope of the LSD project.

1.3.3 WP3 – MEA design (Lead: DPS)

The DPS MEAs have been extensively tested under various conditions. Some of the results from the durability project (See Figure 17 and Figure 18) shows:

- Membrane thinning
- Loss of acid (and hence lower performance due to loss of contact to the Pt/C catalyst and lower conductivity)
- Catalyst degradation (results not shown)

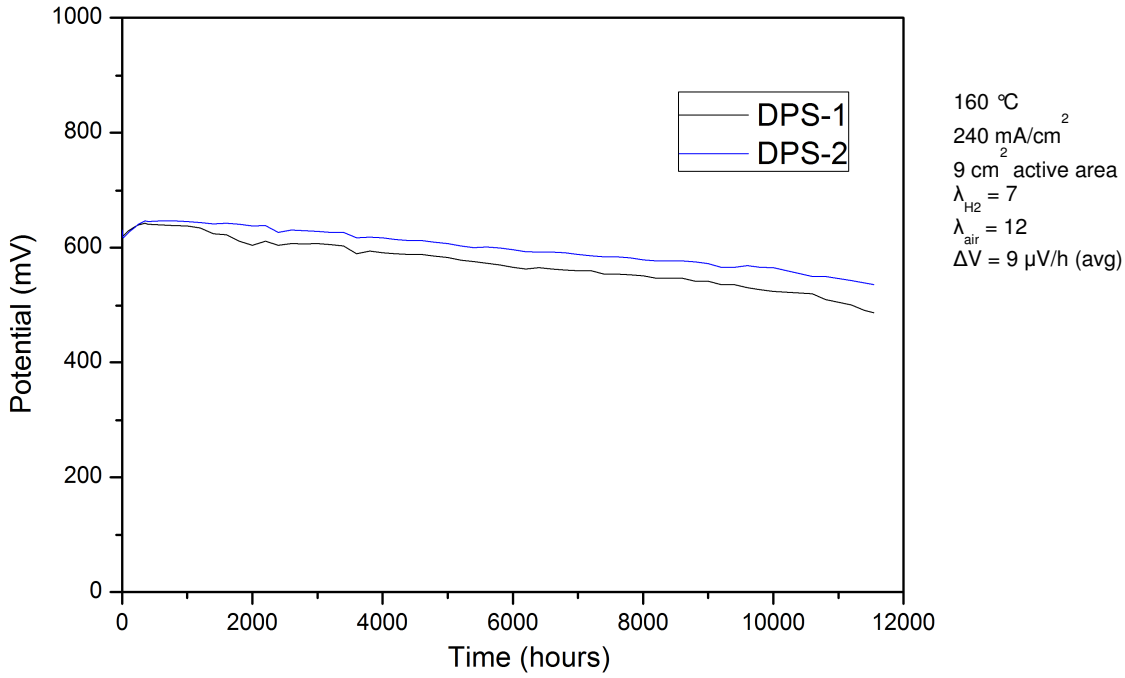

Figure 17: MEA test under constant current conditions.

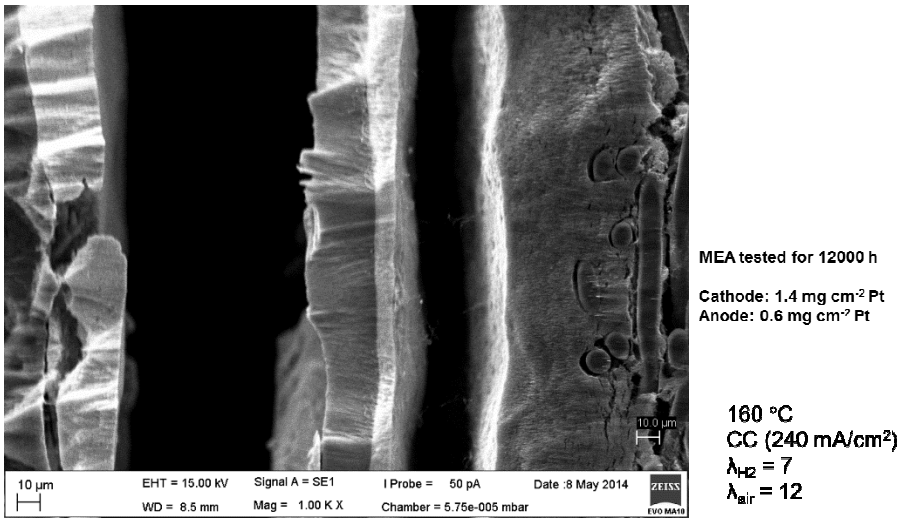

Figure 18: SEM investigation of a MEA cross section. The MEA has been tested for 12000 h (same MEA configuration as in Figure 1).

To achieve a predicted lifetime of +20.000 will require:

- A more stable (or thicker) membrane
- Higher acid doping and/or improved acid management
- More stable catalyst layer (the improved catalysts are being addressed in a number of other projects)

Results from experiments with thicker membranes and higher acid content are shown in Figure 19.

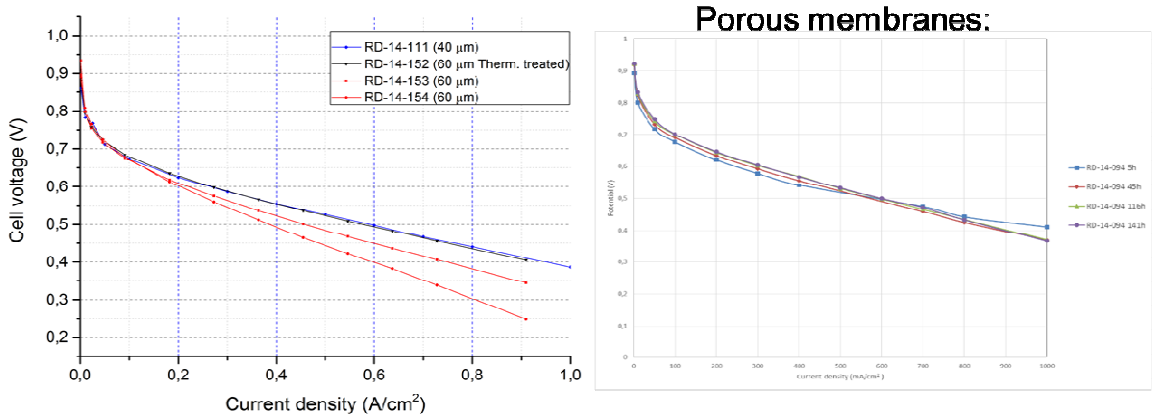

Figure 19: Results from experiments with thicker PBI membranes (left) and higher acid doping levels (right). Test conditions: 160 ℃, λH2 = 1.5, λair = 2.5, 25 cm2 active area (G55).

The thicker membranes generally shows higher resistance, except for the thermally treated membranes. Introducing 20% pores in the membranes results in a doubling of the doping level (Figure 19 left).This results in good performance when combined with a more hydro-phobic catalyst layer, whereas the standard catalyst layer is completely flooded with acid and showing poor performance (results not shown).

Furthermore, investigations of the impact of various test methods on the MEA durability have shown that exposing the MEA to high current densities (even for short durations during e.g. polarization curves) causes degradation.

Thermally treated membranes were chosen as a possible solution to the challenges described above. A process for manufacturing and handling of such thermally treated PBI membranes has been developed and the process and operating conditions has been described in a SOP.

The durability of the optimized DPS MEA design based on the thermally treated membranes has been tested at DPS and two collaboration partners (within the CISTEM project, which aims at demonstrating of the FC part of the LSD project). The results (Figure 20 and Table 2) demonstrates a degradation rate of <3 µV/h, meaning that a projected lifetime of >20.000 is realistic under steady state operation.

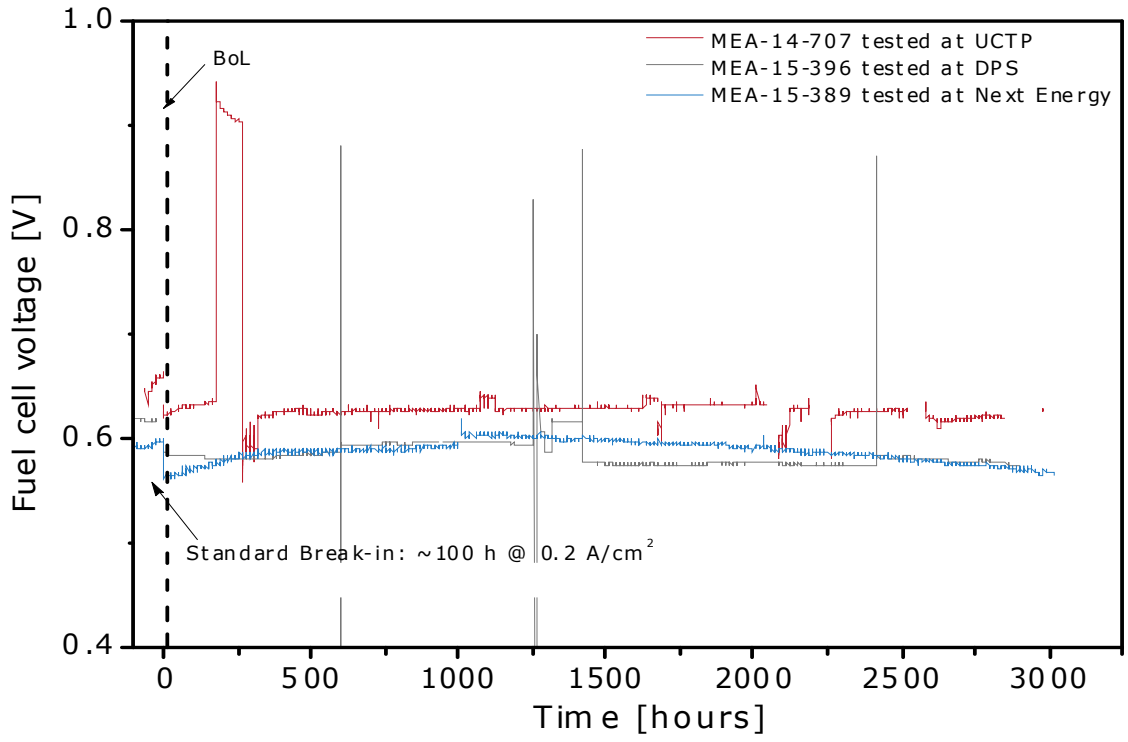

Figure 20: Durability testing of Dapozol MEAs. T=160 °C, 0.3 A/cm2, λH2/λAir=1.5/2, p=ambient pressure, BoL=beginning of life, serpentine flow field, 21 cm2 MEA active area.

Table 2: Degradation rate over time at 0.3 A/cm2.

MEA-14-707 (NE)	+14.2 µV/h	+2.0 µV/h
MEA-15-389 (UCTP)	+3.8 µV/h	-0.9 µV/h (2.800 h)
MEA-15-396 (DPS)	-5.3 µV/h	-4.7 µV/h (2.900 h)

The "abrupt" decrease in performance at ~1400 h of the MEA tested at DPS is due to a period of fuel starvation (12 h). Afterwards, the performance seems stable again.

Electrode and MEA manufacturing:
DPS has manufactured a number of different MEA configurations for WP 1 and 2.

1.3.4 WP4 – FC design (Lead: DPS)

The test of the large MEA design has been tested as part of the CISTEM project through a number of short and full stacks. The target power of the stack is 5 kW_{el}, meaning that a 20 kW system will consist of 4 stack modules. The MEA design for the CISTEM project has been finalized (See Figure 21). An active area of 200 cm^2 results in a stack having 94 MEA's and a power output of 5 kW (a stack voltage of 66 V and 80 A). The resulting MEA dimensions are shown in Table 3.

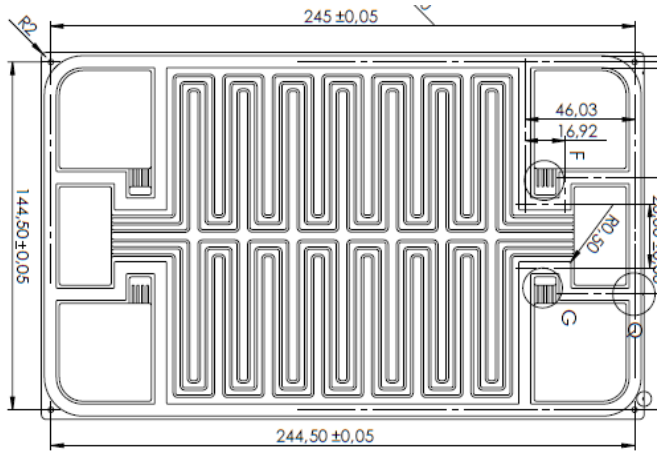

Figure 21: Design of bipolar plate used in the 5 kW stack for the CISTEM project. The active area of the MEA is 200 cm2.

Table 3: MEA dimension for a 5-10 kWel stack module operating at a voltage of 48 or 72 V. IRD has a HTPEM stack design for this size MEA (developed in the FURIM EU project).

Module voltage (V)	48	48	72	72	CISTEM
Module power (kW)	10	5	10	5	5
Cell voltage (V)	0,7	0,7	0,7	0,7	0,7
Cell curent density (A/cm2)	0,4	0,4	0,4	0,4	0,4
Module:					
No of MEA's	69	69	103	103	94
Area of MEA (cm2)	521	260	347	174	200
Comments:		Furim		Std.	

DPS has developed a size flexible manufacturing method, which will enable the manufacturing of even larger MEA's without the cost of expensive tools. Furthermore, this process will enable DPS to manufacture MEA's in costumer's specific sizes without having to invest in expensive tools.

The impact of the degree of CO_2 clean-up on the H_2 utilization has been evaluated (See Table 4).

Table 4: Calculations of the H2 utilisation based on different inlet and outlet gas compositions.

	Gas composition - H_2/CO_2								
Inlet composition (%)	90/10	95/5	99/1	90/10	95/5	99/1	90/10	95/5	99/1
Outlet composition (%)	20/80	20/80	20/80	25/75	25/75	25/75	30/70	30/70	30/70
H2 utilisation	97,2%	98,7%	99,7%	96,3%	98,2%	99,7%	95,2%	97,7%	99,6%

The results in table 3 shows that it is possible to achieve a quite high H_2 utilization (97.2%) even without complete CO_2 clean-up. However, the impact of the actual fuel composition (H_2/CO_2) on the FC performance has not been investigated.

1.3.5 WP5 Hydrogen storage and separation (Lead CISMI and Accoat)

Introduction

Storage of large amounts of pure pressurized hydrogen is associated with a considerably risk of explosion in case of failure or leakage. Failure to address this safety issue would be expected to increase the necessary safety precautions and limit the acceptable locations.
As part of this project we have developed a novel storage concept utilizing CO_2 as an inert buffer gas which significantly reduces these limitations. The CO_2 is only added once to the system, but it is necessary to separate the hydrogen from the CO_2 before its oxidation in the fuel cell. In this chapter we describe the proposed storage parameters and possible solutions for the separation technology; the latter is currently a subject of much research and continuous development.

Safety limits

The triangle plot in Figure 22 is used to assess two limits; first the limits of flammability and secondly the range where detonation occurs if the mixture is ignited. The percentage of air is plotted from 100 % (top of diagram) to the bottom (0 % air). Carbon dioxide and hydrogen is plotted to the left and right respectively, so that the bottom baseline indicates the CO_2 percentage in the pressurized container. Note that the diagram and the following consideration correspond to compressed gases released to air at atmospheric pressure.
The right side of the triangle plot corresponds to mixing pure hydrogen with air. The limits of flammability are between 4.1 to 74 % hydrogen (indicated with crosses) while the limits of explosive risk is 19 to 57 % (filled triangles). By introducing CO_2 we are choosing another starting point on the bottom axis. To assess air dilution we follow a straight line to the top of the diagram. It is obviously unsuitable to completely avoid the flammability region, which would require more than 90 % CO_2 dilutant. The risk of explosion can be avoided by choosing a 40:60 molar ratio of hydrogen and carbon dioxide, as indicated by the vertical line in the diagram.

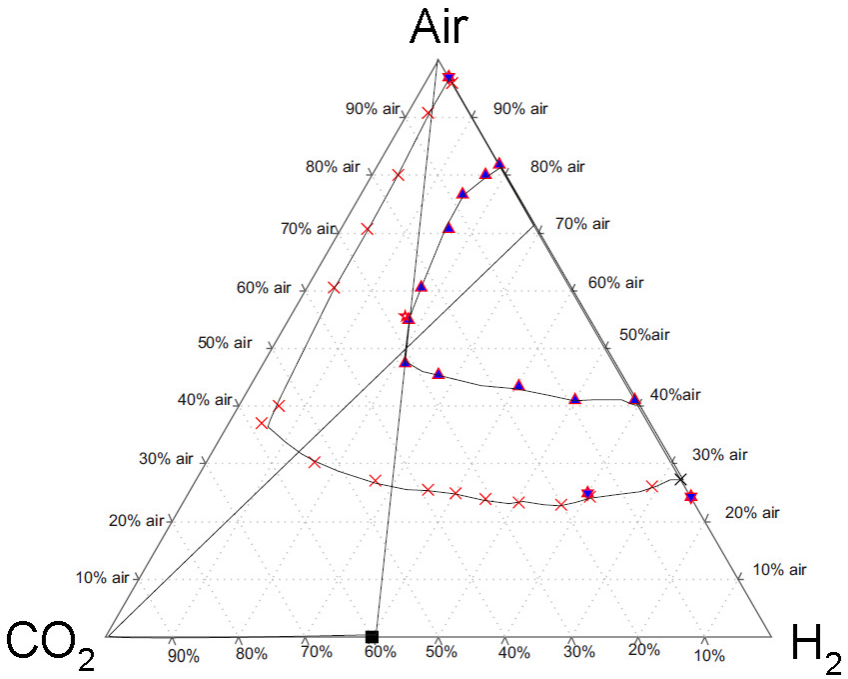

Figure 22: Flammability (x) and explosion (Δ) limits for H2/CO2/air mixtures

Hydrogen storage

In the initial concept, it was assumed that the storage tank should be kept at 40°C. The rationale was that the critical point for CO_2 at 31.1°C and 73.8 bars should be superseded by the conditions chosen for the storage tank, thereby ensuring that the H_2 and CO_2 were com-

pletely miscible. In the study of the available experimental data it is observed that the critical point for mixtures of CO_2 with significant amounts of H_2 is displaced to lower temperature and higher pressure, but data for H_2 above 20 mole% is not available. This behavior is indicated in Figure 23. It is favorable to lower the temperature to ambient temperature to reduce the energy consumption for the operation of the tank and the load on the heat exchanger. It is unfavorable to increase the pressure much above 100 bars, but a composite of literature data plotted in Figure 24 shows that it is not necessary to reach the supercritical region. The figure shows a plot of temperature vs hydrogen mole% (in CO_2) for H_2: CO_2 mixtures at 102 bars. The best fitted line indicates the limit below which a liquid phase appears. A 40 mole% hydrogen mixture at 102 bars separate into two phases below 280 Kelvin (8°C) which is acceptable.

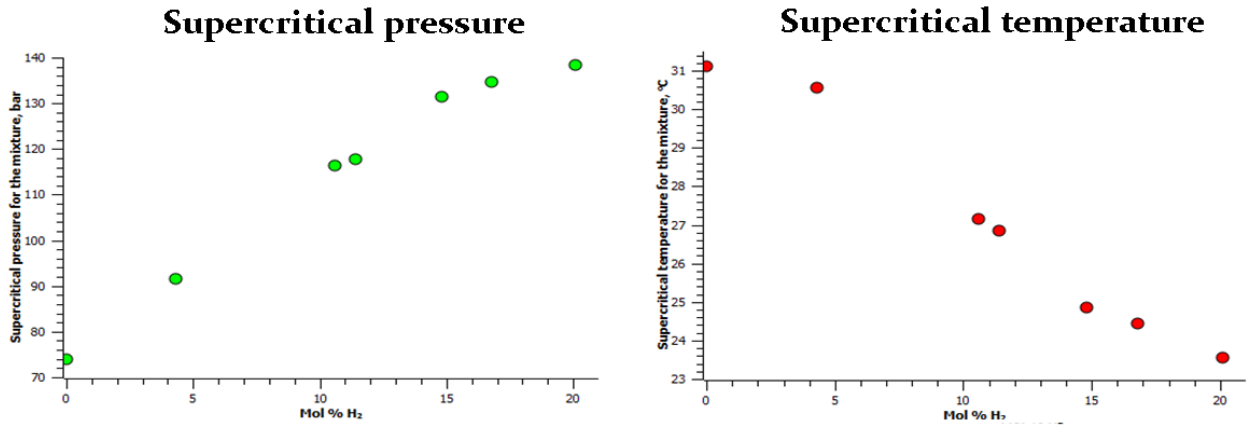

Figure 23: Supercrtitical pressure (left plot) and temperature (right plot) for mixtures of hydrogen and carbon dioxide. Adapted from Ke et al (2001)1.

[1] Ke, J. et al., 2001. How Does the Critical Point Change during a Chemical Reaction in Supercritical Fluids? A Study of the Hydroformylation of Propene in Supercritical CO 2. Journal of the American Chemical Society, 123(16), pp.3661–3670.

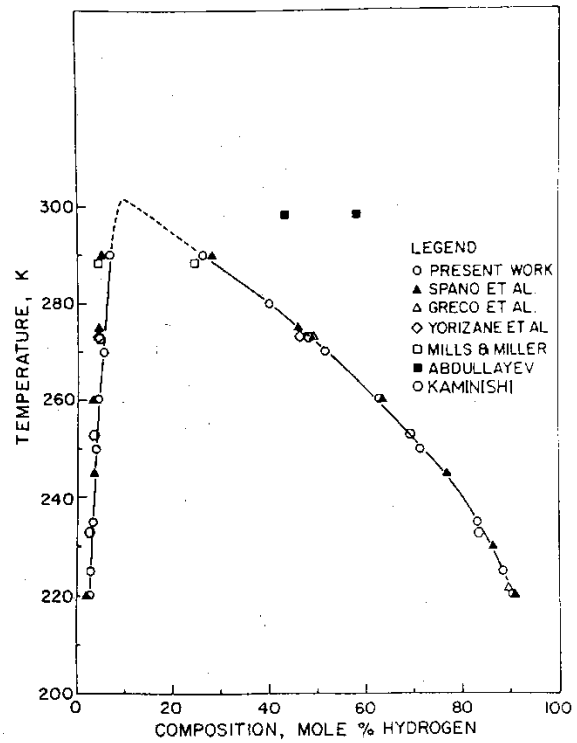

Figure 24: Phase diagram for hydrogen and carbon dioxide gas mixtures at 102 bars and varying temperatures. Below the fitted line the mixture separates into a liquid and gas phase. From Tsang and Streett (1981).

In the simulation of the tank during hydrogen consumption in the fuel cell, it is seen that the pressure will drop in the tank if no further action is taken. It was therefore suggested that the separated CO_2 will be directed back into the storage tank in order to maintain the total pressure. This idea has been incorporated into the process diagram in Figure 25. To retain the 40:60 composition of the gas taken off the tank, the pure CO_2 will be located below a flexible barrier (balloon) located inside the tank. Material that theoretically can be used for this barrier and that can withstand the chemical environment has been found to be commercially available.

The design results in a partial compensation for the removal of hydrogen from the tank. The remaining volume deficit can be compensated either from a CO_2 storage tank or by a second flexible barrier in the tank. Behind this water is pumped into the tank to maintain the 100 bar pressure. In the situation where the tank is completely emptied for hydrogen the latter requires 15 m^3 water to be pumped into the tank. The work performed by an ideal pump moving 15 m^3 to a pressure of 100 bars is 41 kWh. This work is to a large extent compensated by the pressure drop for the purified hydrogen where 100 bars initial storage pressure is reduced to 3 bars at the entrance to the fuel cell.

Separation

Hydrogen is an important chemical that is principally produced by steam reforming of hydrocarbons, followed by the water-gas shift reaction. This results in a binary gas mixture of hydrogen and carbon dioxide. A similar process is utilized in the pre-combustion in an Integrated Gasification Combined Cycle (IGCC) coal plant, producing a mixture of H_2 and CO_2. The latter is then separated and sequestered to lower the CO_2 emission from the plant. Consequently, an economical separation of hydrogen and carbon dioxide is an important and a much researched problem.

This project can to a large extend apply the technologies developed for the aforementioned use directly. Actually, the present project has several benefits in design related to the gas separation when compared to the mixture produced in an IGCC power plant;

a) The hydrogen and carbon dioxide gas mixture does not contain impurities and corrosive gases which typically impose greater material cost and demand service/replacement. This also expands the possible separation technologies.

b) The gases are already highly compressed at 100 bars. A high starting pressure is beneficial for the separation methods.

c) Compared to other gas separations, the target separation goal of 90%+ hydrogen delivered to the fuel cell is modest, and a high hydrogen capture rate (low H_2 concentration in separated CO_2) is not critical, because the CO_2 rich stream gas is recycled in the system.

d) The gas mixture is at ambient temperature and a source of heat is available (spare heat from the fuel cell) which is often beneficial in the separation system.

Taking all the system requirements into consideration this study has examined two separation methods, possibly used in conjunction;

1. Pressure swing
   Pressure swing is a well-known technology in which the differences in physical properties between H_2 and CO_2 is utilized. CO_2 is condensed at high pressure and low temperature and separated from the hydrogen rich gas.

2. Membrane separation
   Gas separation using membranes is a widely used technology with a simple design principle; the gases differ in their permeability through a membrane. The separation is driven by a pressure difference across the membrane.

1. Pressure swing

The first proposal for separation of the storage gas is to bring the gas mixture out of the supercritical region in a pressure swing system. This will result in a phase separation into a gas phase and a liquid phase. Following Tsang and Streett (1981) the cooling of a 40:60 mole-% H_2 and CO_2 gas mixture to 230 K (-53°C) at 100 bars will result in a liquid phase containing 4.1% hydrogen and 90.5% in the hydrogen rich gas phase. The division of material between the two phases leads to 58.5 mole percent in the CO2 rich liquid and 41.5% in the hydrogen rich gas phase.

Figure 25 below shows a diagram of the storage and separation system using pressure swing. The storage tank to the left in the figure contains two bags. The first is storing excess CO_2 when the system is not fully loaded with hydrogen. Eliminating the bag would dilute the hydrogen and increase the separation cost. The other bag contains water that can be pumped into the main storage tank to keep the pressure supercritical at 100 bars at all times. The volume outside the two bags is used for storage of the H_2 and CO_2 mixture.

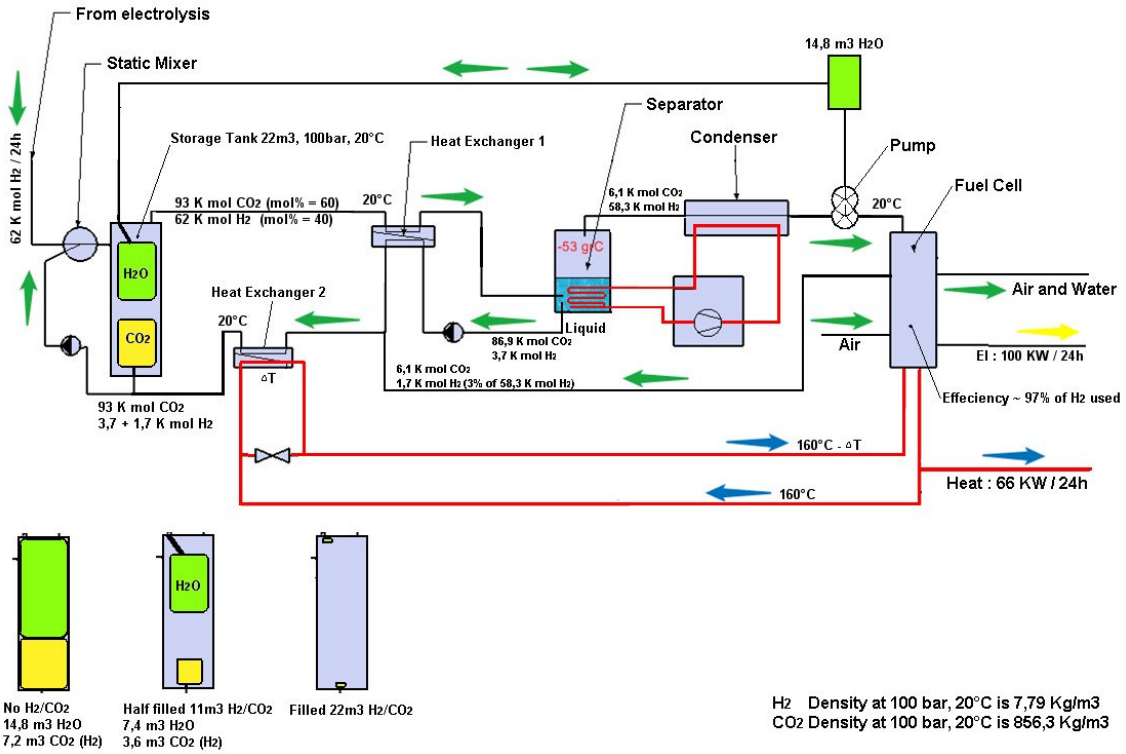

Figure 25: Complete storage and separation system based on pressure swing

The model system in Figure 25 has a capacity of 124kg of H_2 input for 24 hours. This results in an output of 100 kW of electricity generated by the fuel cells. Of this, 10 kW of electricity is used for refrigeration, and 2 kW of electricity is used for pumps. Therefore 88 kW will be generated by the system. At the same time 66 kW of heat is generated.

Calculation of storage requirements

The requirement of 124 kg of hydrogen (60.5 Nm^3) is equal to 61500 mole of hydrogen. A mixture of 40% hydrogen and 60 % CO_2 should accordingly be loaded with 4060 kg CO_2. We have assumed that we are working with a supercritical mixture. Selecting 100 bars and 20°C it is possible to calculate that the density of CO_2 is 856 kg/m3. The space taken up by the supercritical CO_2 is 4.74 m^3. In the original proposal a tank of 18 m^3 was described. Using a 40:60% mixture increase the volume to 22 m^3.

Based on the demands of the storage tanks it is more economical to divide the gas storage between smaller, slimmer tanks instead of a single large tank. Based on a price offer from Dana-Tank four tanks with the required total capacity would cost 1.34 million DKK. The remaining system cost is shown in the price list below. The total cost of the system is estimated at 2.4 million DKK. Most of the price is attributed to the storage tanks.

The sketched system has parameters for a mixture of H_2/CO_2 = 40/60, but if this mix is changed to H_2/CO_2 = 80/20 then the tank capacity will drop from 22m^3 to 16,2m^3. This will significantly decrease the cost of the system since the storage tank is a large part of the 2,4 million DKK. Since the capacity of all components is reduced the total price will drop to below 2 million DKK.

2. Membrane separation

There are several membrane materials for gas separations that rely on different separation principles. It is important to note that while in the literature some of these have shown remarkably high separation characteristics for H_2 and CO_2, they are often limited by technical

or economical disadvantages with the fabrication of practical modules on a larger scale. The dominating technology for gas separation is polymeric membranes, which are the focus in this project in the experimental work with carbon hollow fibers and the commercial alternative modules discussed hereafter.

Membranes can be either H_2 or CO_2 selective. The efficiency of polymeric CO_2 selective membranes are typically optimal at ambient or cold temperatures, while the H_2 selective membranes are typically operated at elevated temperatures of 100-150°C. The CO_2 selective polymeric membranes also typically have higher trans-membrane flow compared to the H_2 selective membranes. These factors suggest CO_2 selective membranes should be preferred, but other considerations should be taken into account. The most important is the composition of the gas mixture and which gas should preferably exit as the low pressure component (permeate), in our case hydrogen at 3 bars. Sometimes a combination of CO_2 and H_2 selective membranes is preferable.

A few large corporations produce membrane modules suitable for hydrogen and carbon dioxide separation. These include Air Products (PRISM®), Air Liquide (MEDAL™) and MTR (Proteus™ and Polaris™). The latter (MTR) produces both H_2 and CO_2 selective membranes with high performance characteristics (Their CO_2 selective Polaris™ module has a CO_2/H_2 selectivity of 10 and permeance of 1000 GPU[2] while the H_2 selective membranes have a selectivity of 15 and permeance of 300 GPU at 150°C).

In dialog with MTR two solution strategies for the present separation challenge were considered; combining membrane separation with pressure swing or using a membrane-only system. Based on model results both solutions could improve the energy efficiency compared to the pressure-swing model in Figure 25, but using a membrane-only setup with hydrogen selective membranes has significant benefits. The simulated separation system below is based on Proteus™ hydrogen selective membranes from MTR.

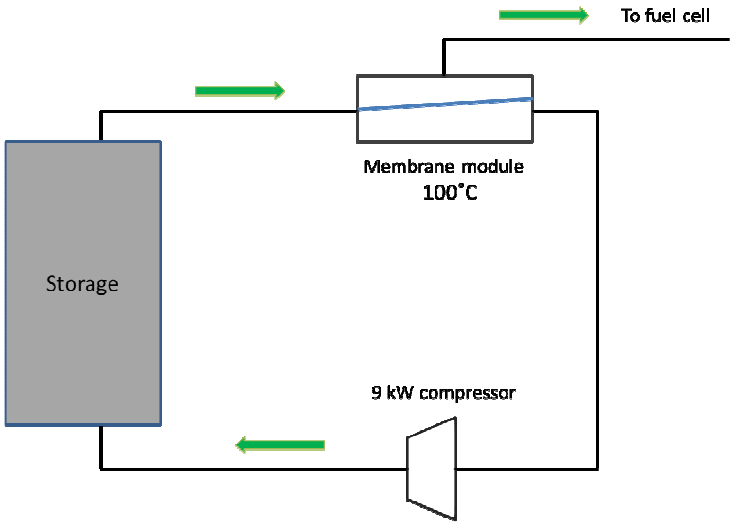

Figure 26: Conceptual process diagram of a membrane separation system

Figure 26 above shows how the gas separation can be performed in one step using a hydrogen selective membranes system. The 40:60% H_2/CO_2 gas feed enters the module at 100 bars and exits in two gas streams. The permeate exit as the low pressure stream at 3 bars

[2] One Gas Permeance Unit (GPU) = 10^{-6} $cm^3(STP)/(s \cdot cm^2 \cdot cm\ Hg)$

and contains 90 % H_2 which can be fed directly into the fuel cell. The retentate has a slight pressure drop and is mostly CO_2 with some residual H_2. It is recompressed with a turbo pump back into the storage tank at a power draw of 9 kW. The membrane module is preferably maintained at 100°C to improve performance. In this setup a very minor membrane area is necessary, about 10 m^2. This is half the area of the smallest 20 L module MTR is currently manufacturing. The typical price point of available membrane skids are 3300 DKK per m^2, but given the small module size and high pressure requirements the module would have to be custom made. Because most of the price would be connected to labor and cost of standard pressure components a cost saving is expected compared to the relatively expensive pressure swing components (see price list). The module would be small and easy to install/replace and the heating requirement could be supplied by the fuel cell.

A typical membrane module lifetime is 3 years, but the clean gas stream would expectantly extend this to 5+ years. This estimate is based on continuous operation, further expanding the lifetime of the module in our operating conditions. Compared to the pressure swing solution the membrane system has the added benefit that it is possible to increase the hydrogen content in the permeate gas by adjusting the flow conditions. This optimization is far less desirable in the pressure swing system.

Discussion

A storage and separation system that meets the technical goals has been described. The separation goal can be achieved with a basic pressure-swing system as described in Figure 25. Reviewing the component prices for this system (price list) the total price of 2.4 million DKK is larger than initially expected. Incorporating membrane separation was found to be an attractive alternative and a way to reduce system cost. A system based on commercially available membranes (Figure 26) can achieve the separation goal at a higher efficiency and expectantly lower cost of acquirement. This would unfortunately not lower the cost attributed to the gas storage. To make a considerably reduction in this cost it would be necessary drastically change the storage concept. Abandoning the CO_2 buffer concept and retaining the hydrogen storage would lead to marginal reduction in tank volume. Another possibility would be to chemically convert the H_2 and CO_2 to formic acid or methanol which can be stored as liquids at very low cost. At standard temperature and pressure one liter of formic acid or methanol contains 53 or 99 g of hydrogen respectively, which are approximately 10 and 20 times the hydrogen storage density of the project concept. A small gas tank with backup from the liquid reservoir could be a solution. While it conceptually is clearly attractive, this method is limited by the present catalyst efficiency and also by the energy lost in the chemical conversions. The optimizations of the process required are mostly in the research phase and cannot be evaluated in an economical comparison yet.

Price list

Component	Manufacturer	Specification	Price
Heat Exchanger 1	Alfa Laval	AXP10-10H-F	(Offer) 3.660,- dkr
Heat Exchanger 2	Alfa Laval	AXP10-10H-F	(Offer) 3.660,- dkr
Storage Tank	Dana-Tank, Nylandsvej 9,DK-6940Lem St.	4 tanks of 5,7m^3 H_2O CO_2 and H_2/CO_2 AD2000 & PED 97/23/EC	(Offer) 1.340.000,- dkr
Separator	Custom made		(Estimate) 300.000,- dkr
Condenser	Custom made		(Estimate) 100.000,- dkr
Cooling compressor	Huber / Buch & Holm	32,5kW, 4,5 ton/24h	(Offer) 410.000,- dkr
Water Tank	Custom made	14,8m$_3$ at 100bar	(Estimate) 20.000,- dkr
Pump	Cat Pumps, Iversen Trading, Sintrupvej 7, DK-8220 Brabrand	Liquid CO_2 4,5 ton/24h	(Offer) 35.000,- dkr
Pump	Cat Pumps, Iversen Trading, Sintrupvej 7, DK-8220 Brabrand	Liquid CO_2 4,5 ton/24h	(Offer) 35.000,- dkr
Pump	Cat Pumps, Iversen Trading, Sintrupvej 7, DK-8220 Brabrand	Water	(Offer) 5.000,- dkr
Mixer		4,5 ton/24h	(Estimate) 20.000,- dkr
Valves		100 bar	(Estimate) 40.000,- dkr
Tubings and fittings		100 bar	(Estimate) 100.000,- dkr
Total			2.412.320,- dkr

Overview of project work

- Measurements of mixed gas separation on CMS modules from SDU
- Literature study of pressure swing adsorption with ionic liquids
- Literature study on alternative hydrogen storage in methanol and formic acid
- Experimental studies of commercial PDMS membrane modules. The modules could perform the necessary separation but certain performance characteristics were unsatisfactory; it was concluded that coating the PDMS membranes with a thin separation layer would increase selectivity. Additionally, a higher trans-membrane pressure rating would be preferably to ensure better performance. A commercial membrane with these characteristics could conceptually be incorporated in the pressure swing model to reduce the gas separation power requirements.

1.3.6 WP6 – Separation (Lead SDU and Accoat)

The objective was to investigate the feasibility of using membrane technology to remove the CO_2 from a stored H_2/CO_2-mixture before using the purified H_2 in a fuel cell. Assuming a 60 STP m3/h feed stream composed of 90 mol% H_2 and 10 mol% CO_2, a literature study and some initial modelling indicated carbon membranes as the most promising candidate. Hollow fibers were chosen as the membrane configuration, since this minimizes the unit operation space required for a given membrane area.

Carbon membranes are manufactured by pyrolyzing polymer precursors. Based on the literature study, cellulose derived from cellulose acetate was chosen as the precursor for this work. Hollow cellulose acetate fibers were manufactured at NTNU in Norway using a spinnerette as seen on Figure 27. Following an already established procedure, the polymer was mixed with a small amount of PVP, dissolved in NMP and extruded through the spinnerette into a water bath, where the polymer re-precipitated due to solvent exchange. The bore fluid consisted of water and NMP.

Figure 27. Spinnerette setup.

Prior to pyrolysis, the cellulose acetate was deacetylated using a solution of NaOH in 96% ethanol. As the SEM images on

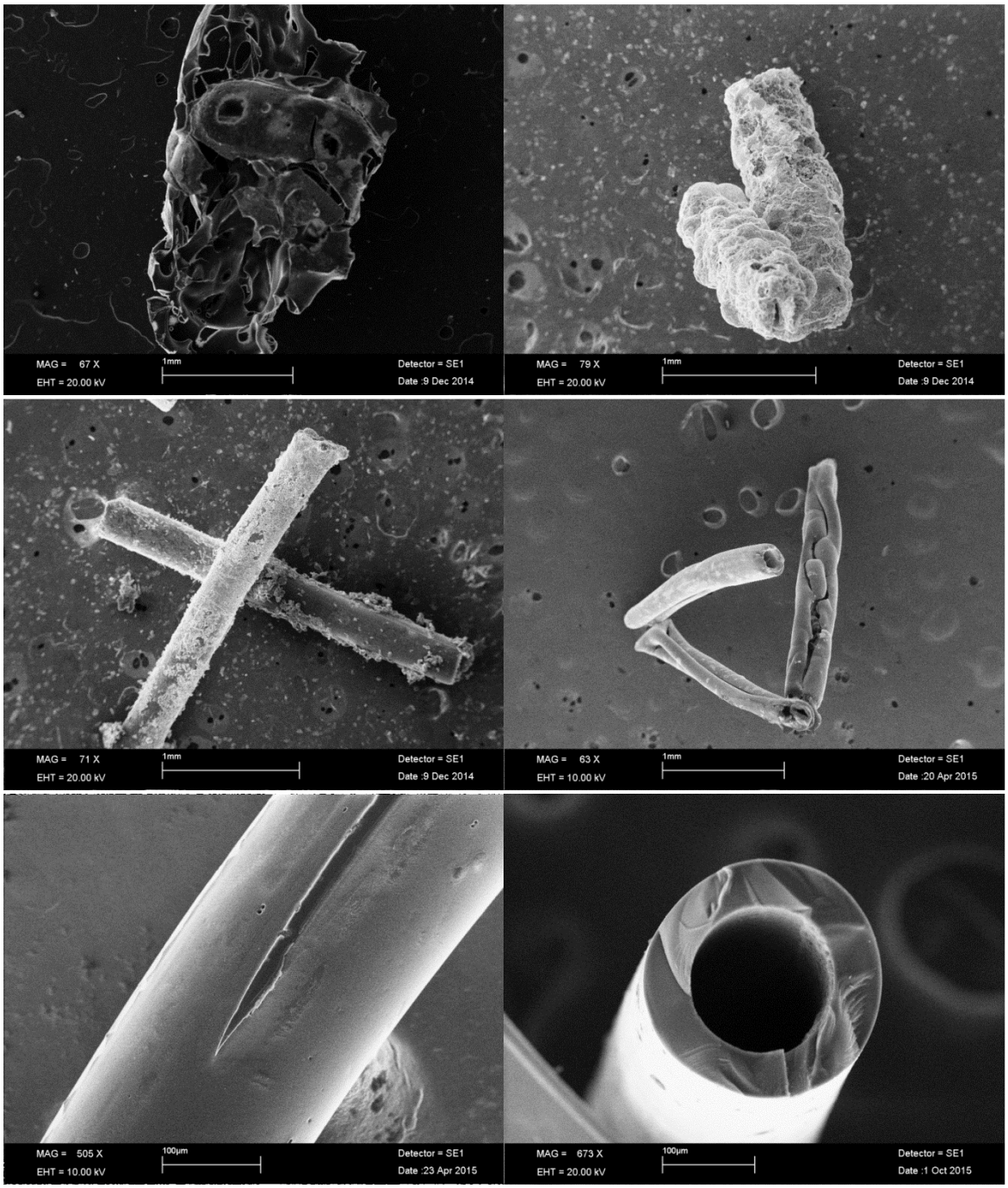

Figure 28 show, the deacetylation time had a significant impact on the structure of the resulting carbon fiber. For all the following pyrolysis experiments, the cellulose acetate hollow fibers were deacetylated for 72 hours.

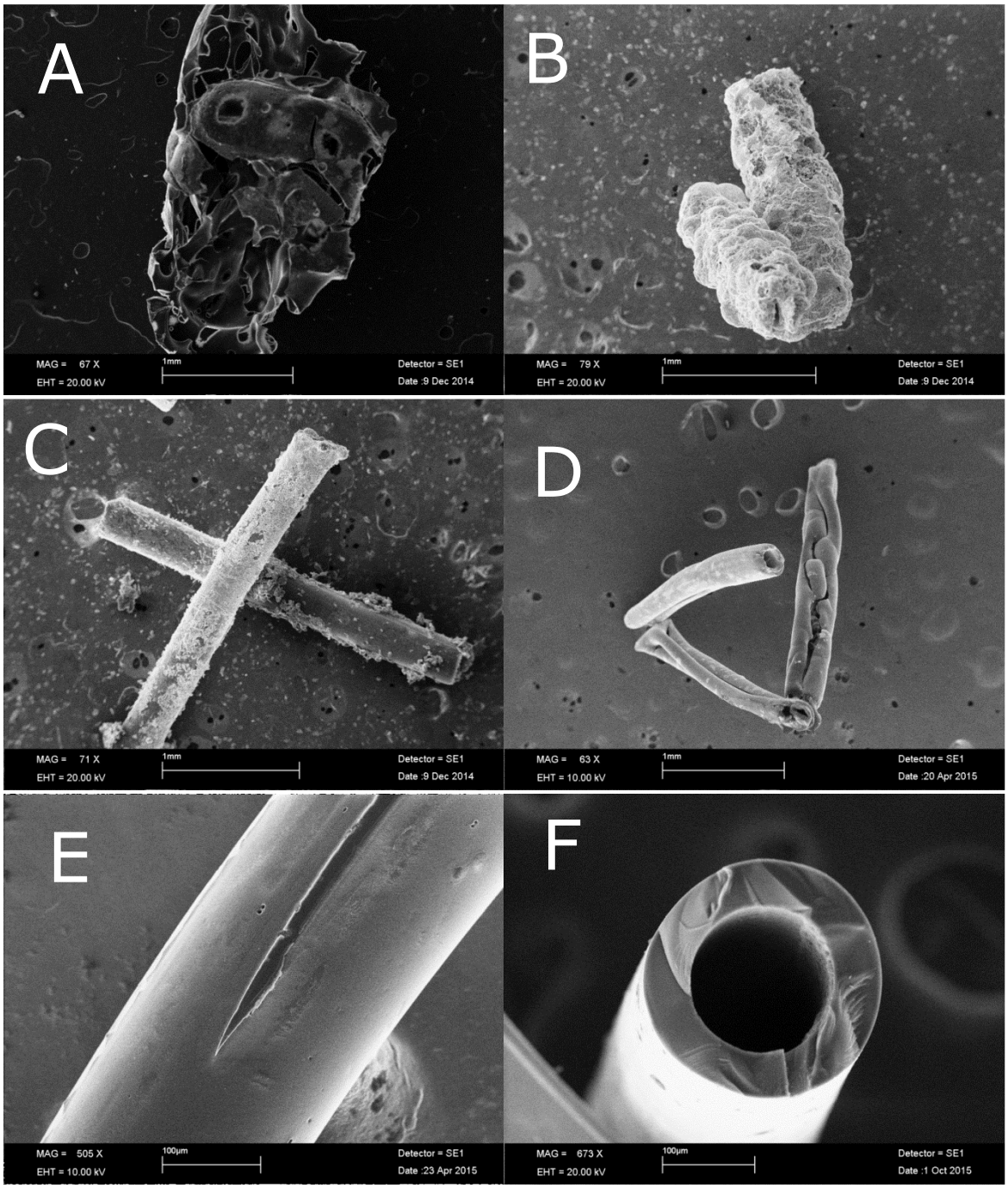

Figure 28. SEM images of pyrolyzed cellulose acetate fibers deacetylated for varying amounts of time. A: 0 hours, B: 2 hours, C: 5 hours, D: 20 hours, E: 48 hours, F: 72 hours.

In order to ensure uniform temperature distribution along the fibers during pyrolysis, a Carbolite tube oven with 3 heating elements was purchased, Figure 29 shows the applied temperature protocol (max temperature was varied). The dwells and the low heating rate (1 °C/min) allow the material to carbonize without creating defects and still retain the hollow cylindrical shape seen on

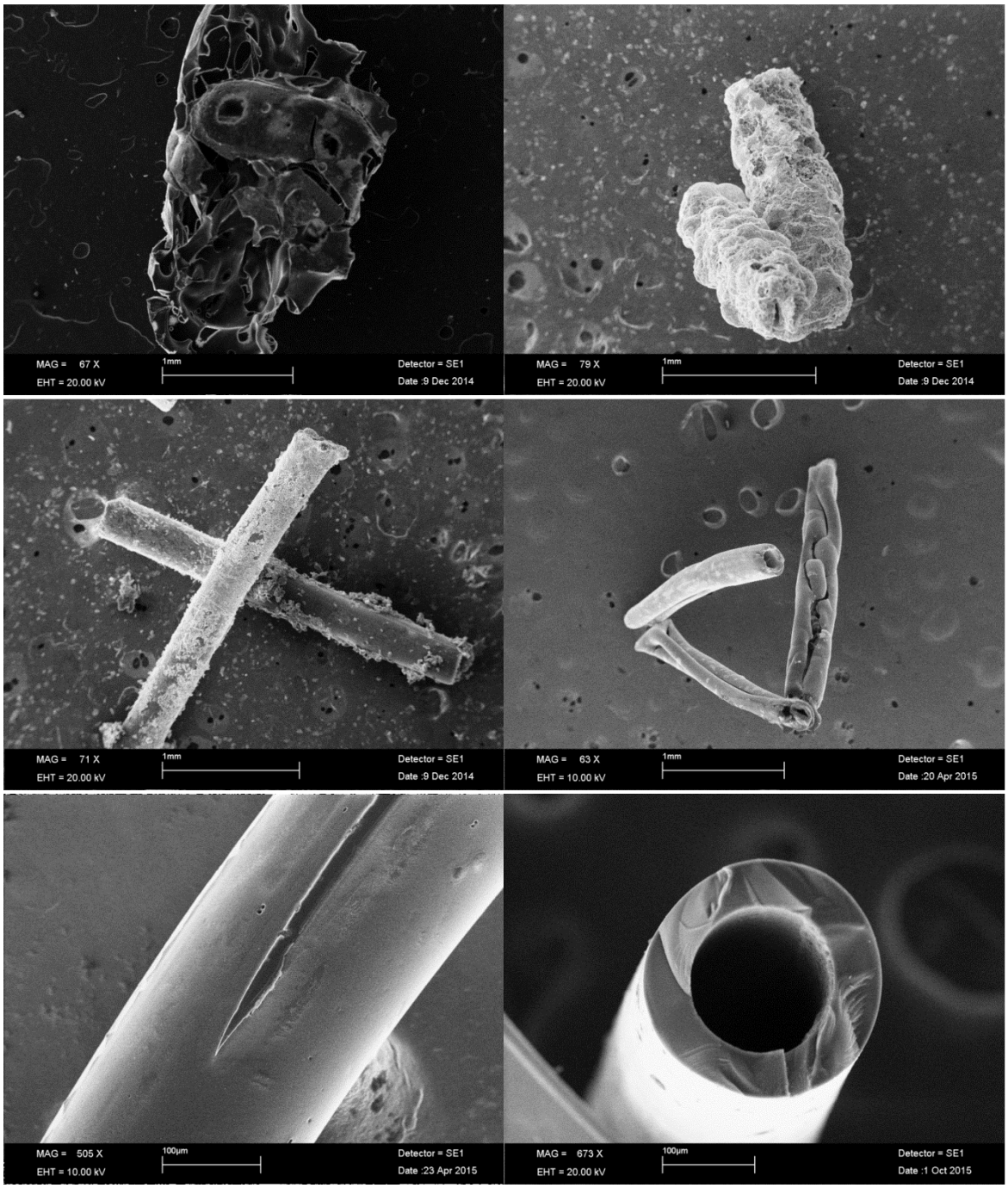
MAG = 67 X
EHT = 20.00 kV
1mm
Detector = SE1
Date :9 Dec 2014
MAG = 79 X
EHT = 20.00 kV
1mm
Detector = SE1
Date :9 Dec 2014
MAG = 71 X
EHT = 20.00 kV
1mm
Detector = SE1
Date :9 Dec 2014
MAG = 63 X
EHT = 10.00 kV
1mm
Detector = SE1
Date :20 Apr 2015
MAG = 505 X
EHT = 10.00 kV
100µm
Detector = SE1
Date :23 Apr 2015
MAG = 673 X
EHT = 20.00 kV
100µm
Detector = SE1
Date :1 Oct 2015
Figure 28 F.

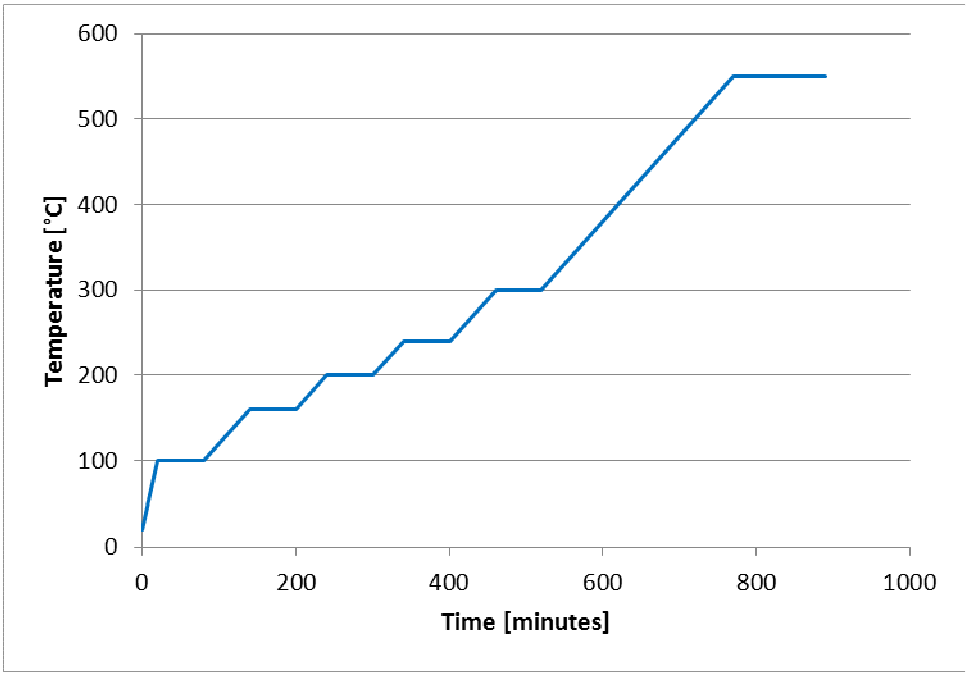

Figure 29. Applied temperature protocol.

The goal was to investigate the effects of temperature and HCl content in the pyrolysis gas on the gas separation performance as well as the mechanical properties of the membranes. Lab scale hollow fiber modules containing 5 of the fibers resulting from the pyrolysis conditions in Table 5 were constructed, an example is shown on Figure 30. The HCl gas was produced in situ by adding concentrated H_2SO_4 to NaCl. To ensure that no water was present in the polymer fiber pores before adding HCl to the pyrolysis gas, it was added once the temperature reached 200 °C for all experiments.

Sample number	1	2	3	4	5	6	7	8	9
Max Temperature [°C]	550			600			700		
HCl in pyrolysis gas (Ar)	0 %	5 %	10%	0 %	5 %	10%	0 %	5 %	10%

Table 5. Applied pyrolysis conditions.

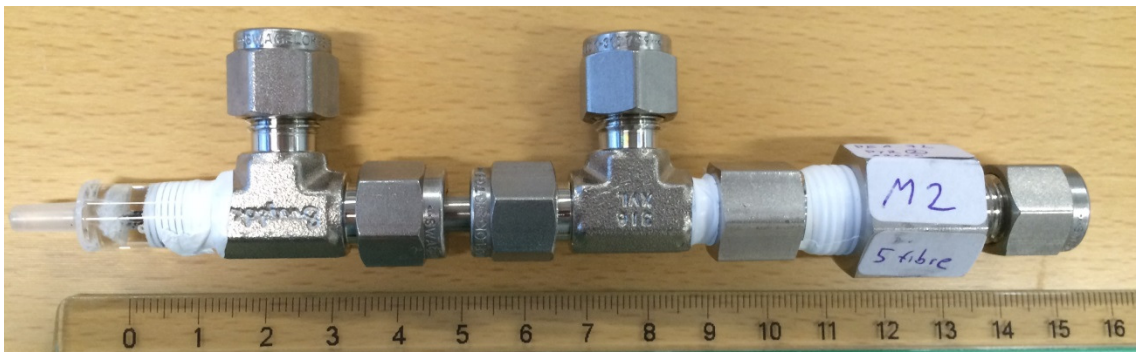

Figure 30. Lab scale hollow fiber module.

Single gas permeability measurements were done for H_2, CO_2, O_2 and N_2 for each membrane module. Since the modules only contain 4-5 cm^2 of membrane area, the expected gas flow rates are too small to be measured reliably with a bubble flow meter. Instead the flow rates were determined by drawing a vacuum on the tube side of the fibers, applying pressure on the shell side and then measuring the rate with which the pressure rises, once the vacuum pump is shut off. The volume of the pressure cell must be known and the derived formula

used to calculate the permeability (Perm) along with an illustration of the setup is seen on Figure 31.

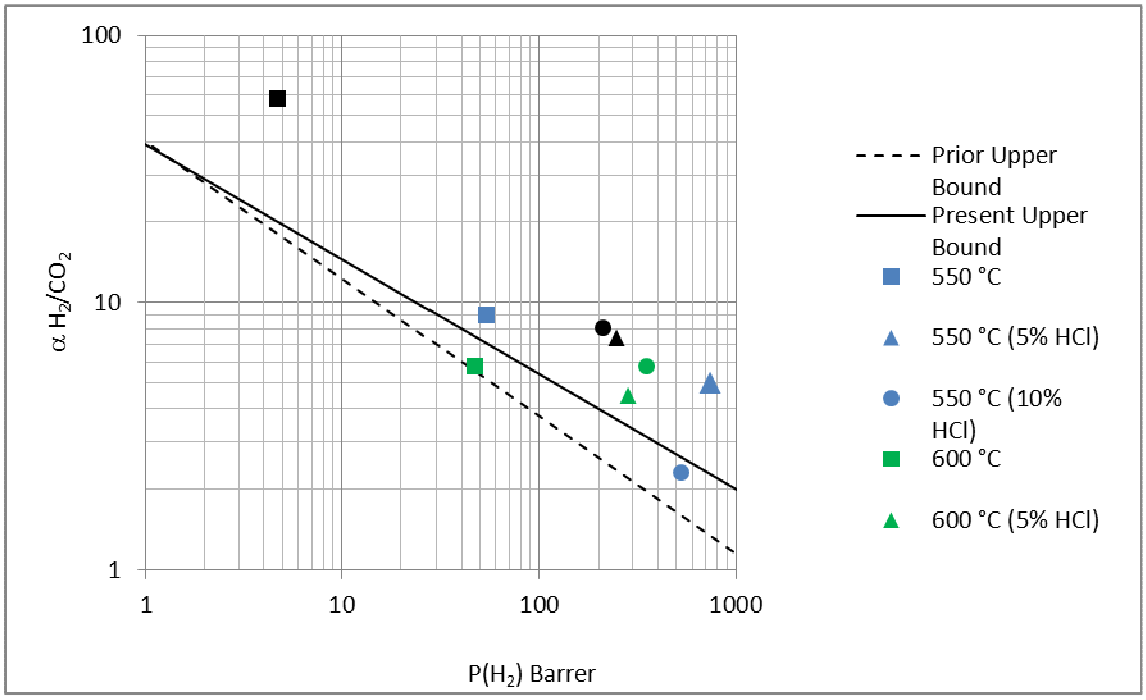

Figure 32 shows the measured H_2 permeabilities and H_2/CO_2-selectivities and Figure 33 shows all the measured single-gas permeabilities.

The mentioned Robeson upper bounds on

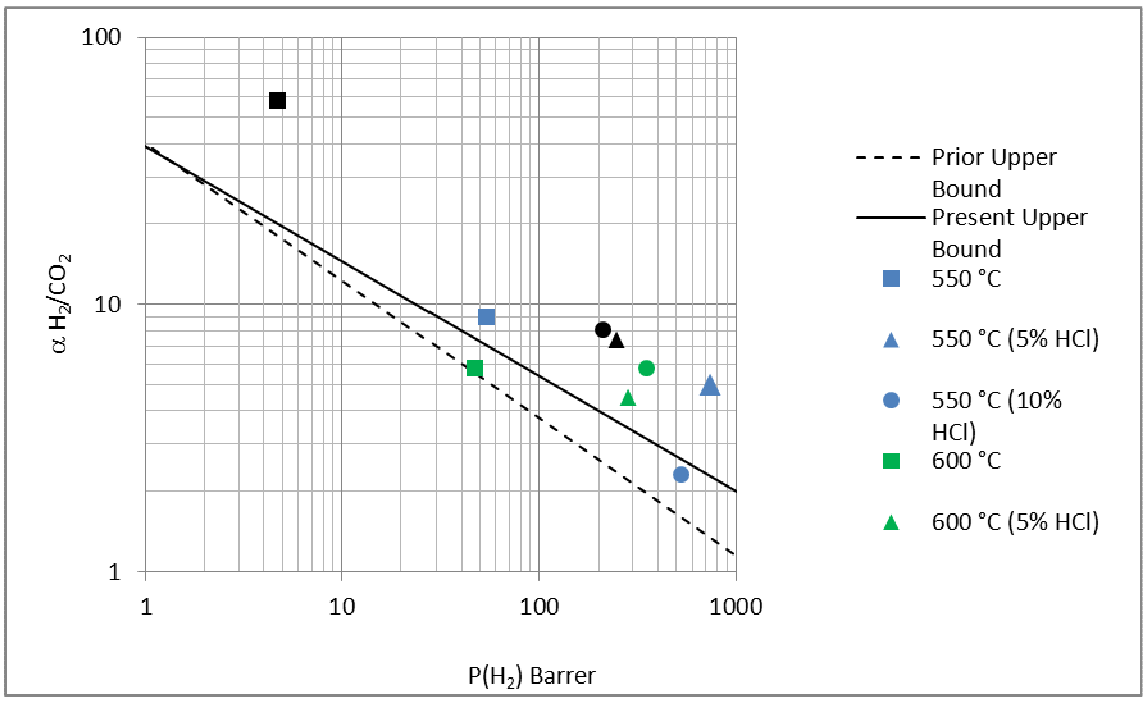

Figure 3 and

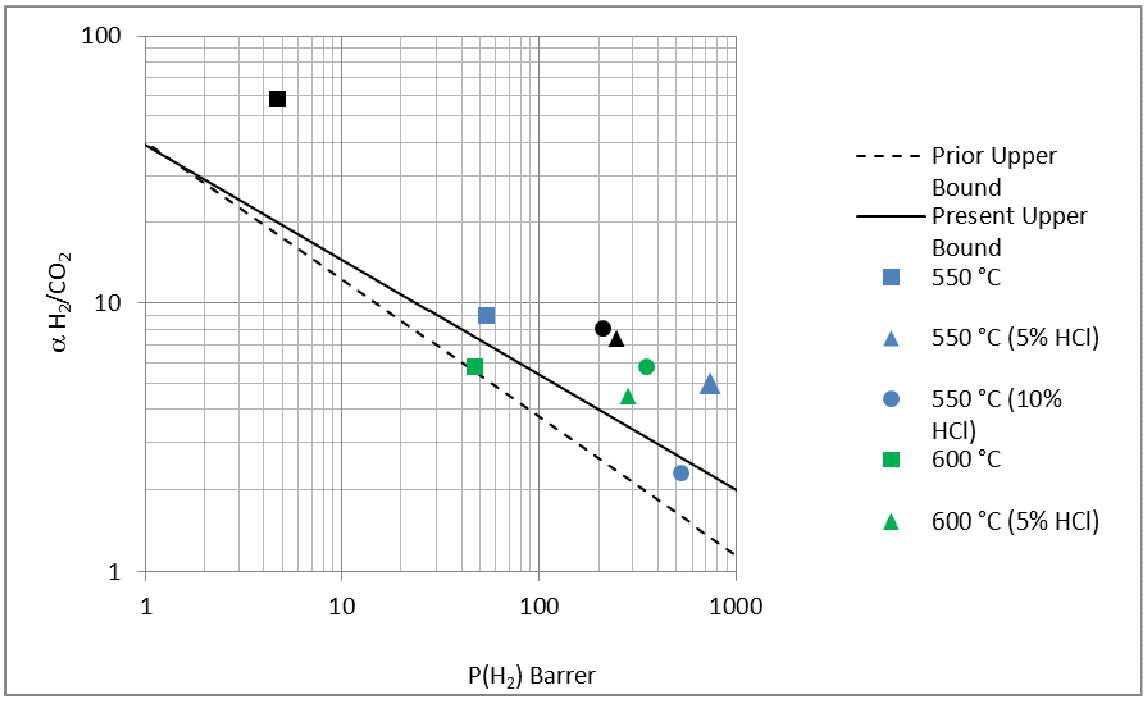

Figure 32 signify the limitations of available membrane materials for a specific gas pair, in this case H_2 and CO_2. They are the result of two large literature studies made by Robeson et al. [1, 2] and are often referenced by authors seeking to compare new materials to already existing ones.

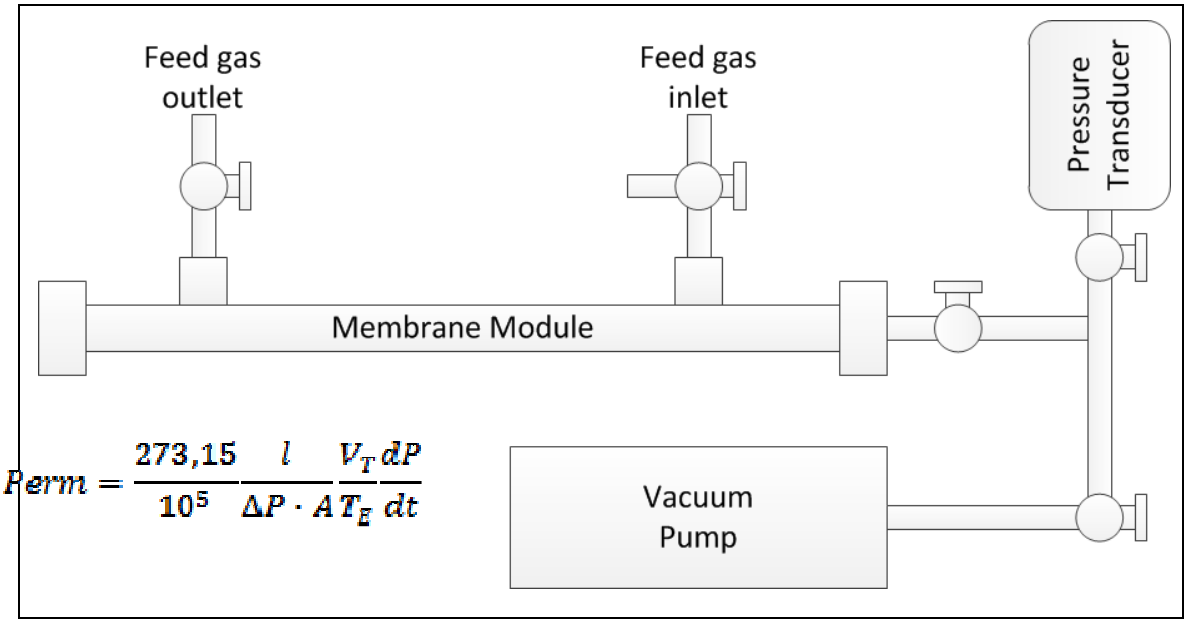

Figure 31. Pressure cell for the determination of gas permeabilities.

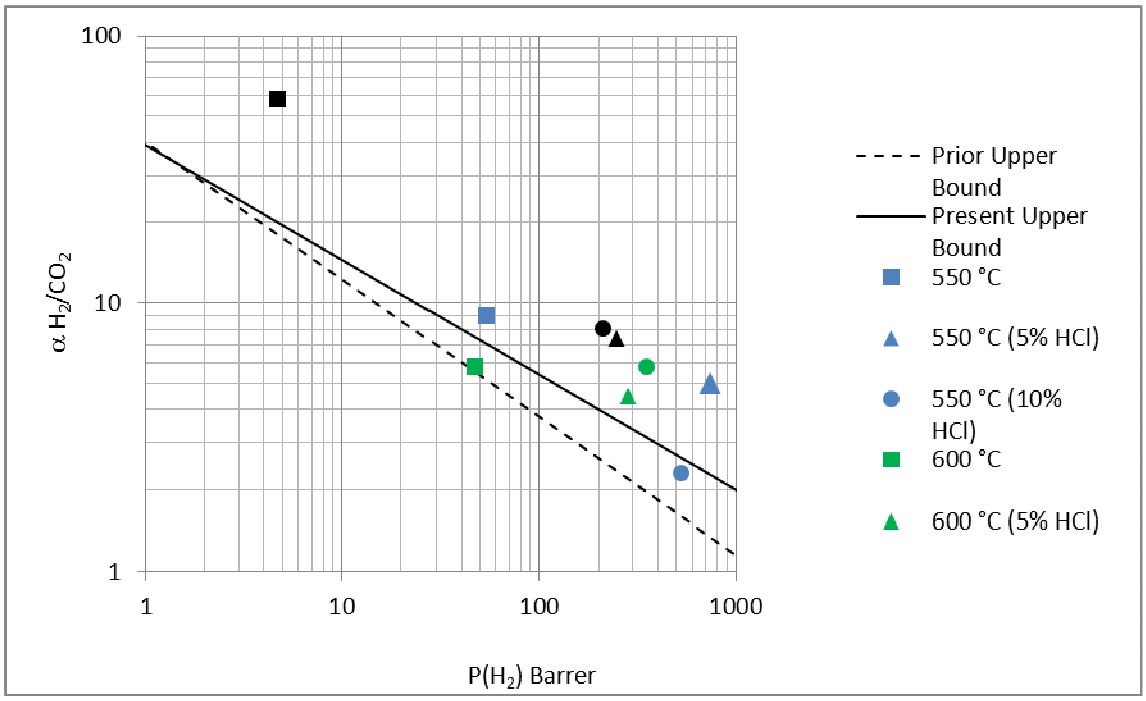

Figure 32. Measured H2/CO2-performance and Robeson upper bounds.

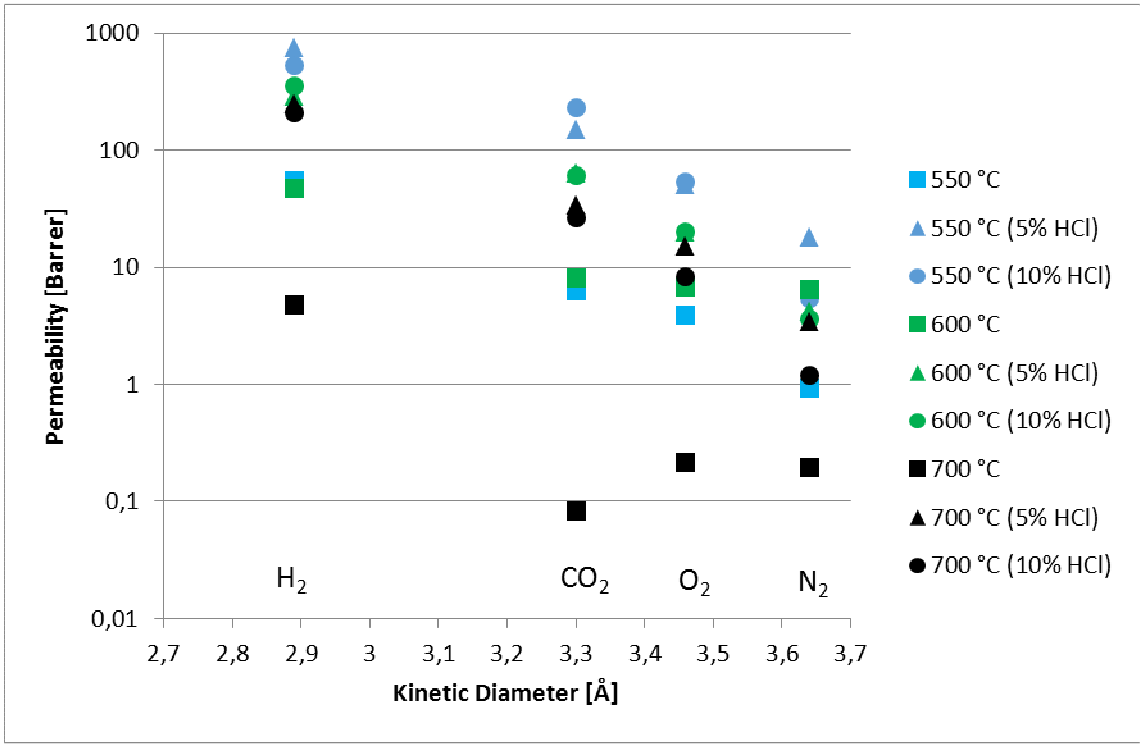

Figure 33. Measured single gas permeabilities.

In order to determine the mechanical properties of the fibers, they were placed in the setup shown on Figure 34 *and pressure was applied from above by lowering a ¼ inch steel tube with a constant speed until the breaking point was reached. The results are shown on* Figure 35.

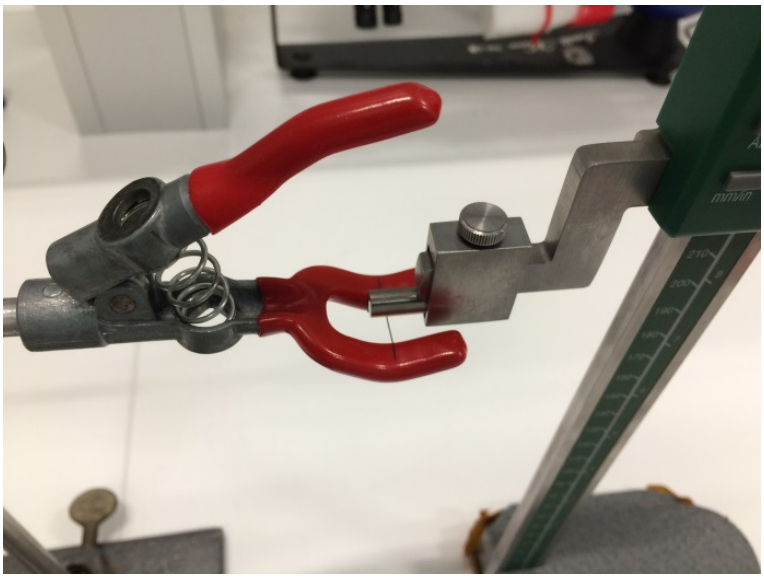

Figure 34. Setup for determining the breaking point of the fibers.

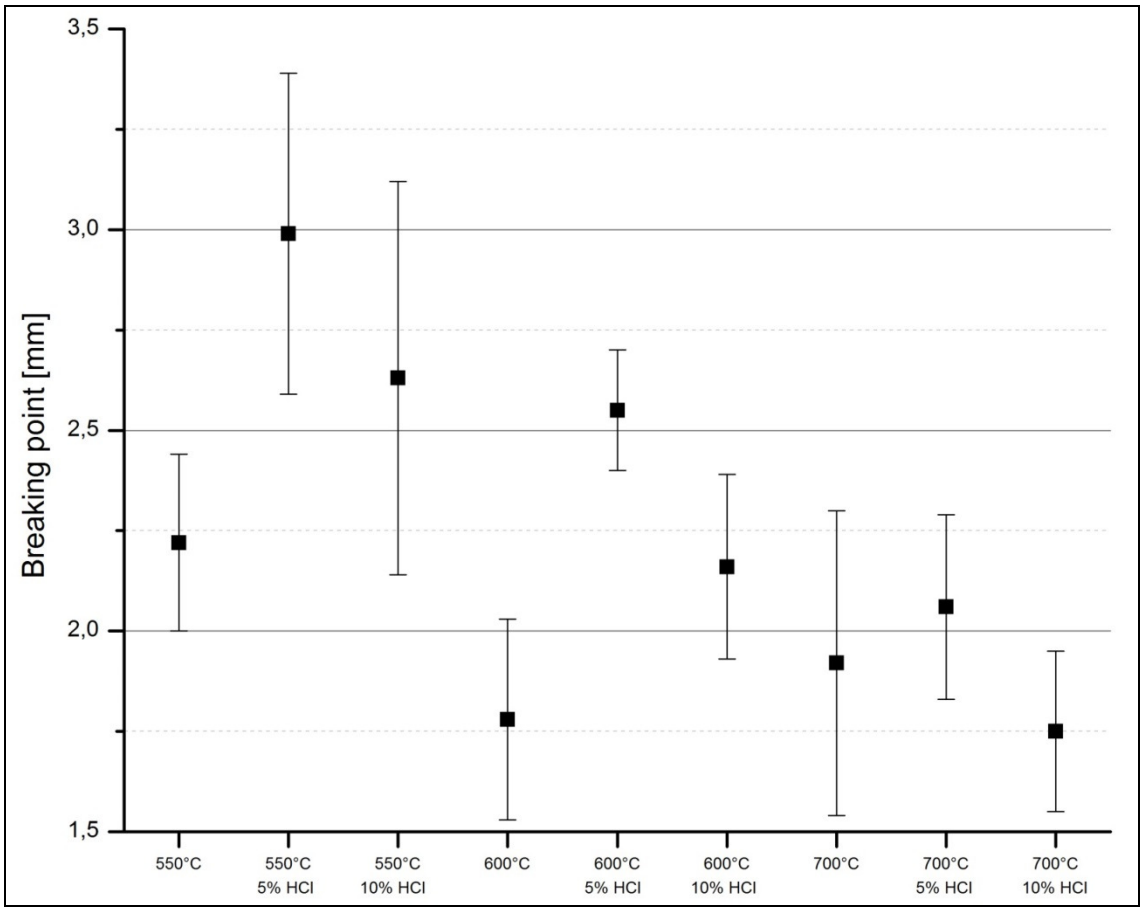

Figure 35. Measured breaking points.

One filter module has been produced using 7 hollow fibers from SDU. Experience about how the fibers are casted into epoxy has been gained. The biggest problem that occurred was capillary effect on the outside of the fibers.

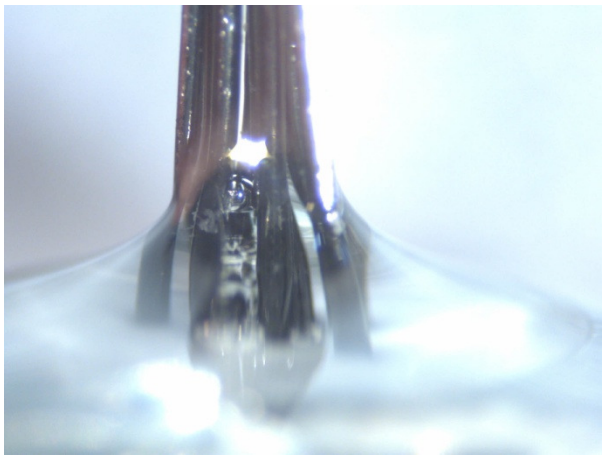

Figure 36: Capillary effect on the outside of the fibers.

This problem can be solved by separating the fibers using a small tread. This is the way commercial available filters are manufactured.

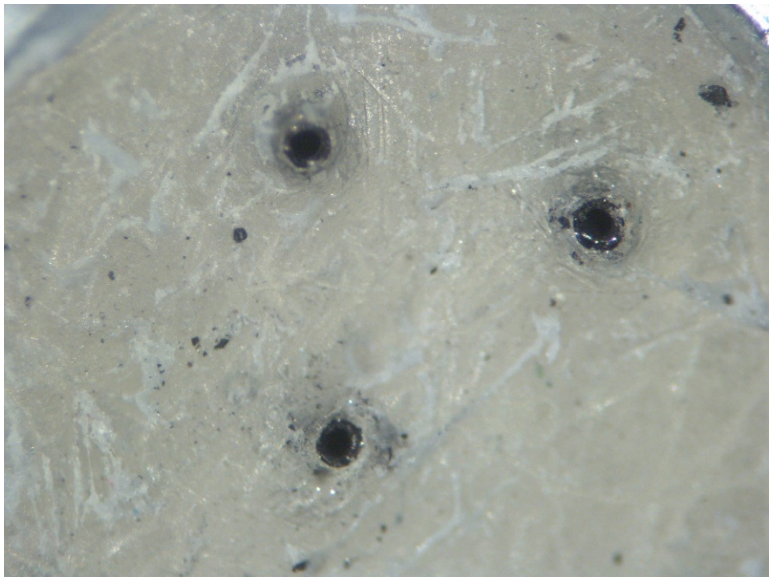

Figure 37: Successfully casted hollow fibers.

3 different methods has been tried of in order to find the best way to make an air tight seal between the inside and the outside of a hollow fiber. Figure 38 shows the chosen method. The ends of the hollow fibers are closed by a high viscos compound. The seal is then casted on top of this using a low viscos epoxy resin. At last is the high viscos compound removed together with a small part of the hollow fiber. The successful result of this method is shown in Figure 37.

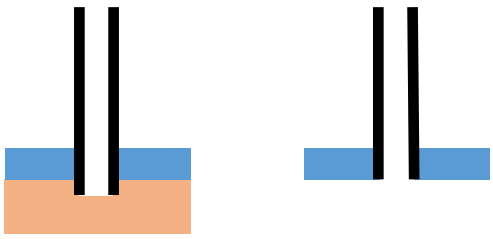

Figure 38: Method of casting a tight sealing

1.4 Utilization of project results

DTU:
The results on oxygen enrichment of air and the effect of CO poisoning on the cathode has resulted in 2 publication, the first one is missing some clarifying measurements, which will be run in the autumn, the second one is currently in review, at International Journal of Hydrogen.

DPS:
The LSD project results have significantly strengthened the potential use of HTPEM for CHP applications and have resulted in:
- DPS participation in the CISTEM project (FCH-JU-2012-1 project no. 325262)
- DPS participation in an application related to large scale demonstration of HTPEM fuel cell based CHP systems using natural gas as fuel (FCH-02-8-2016: Large scale demonstration of commercial fuel cells in the power range of 20-100kW in different market applications).

Furthermore, the project have facilitated the development of a flexible manufacturing setup, which enables manufacturing of large MEAs (>200 cm^2).

CISMI:
Theoretical and practical experience with membrane technology was achieved. The experience will be used in other gas separations for fuel cells.

SDU:
The work done on hollow fiber carbon membranes is expected to result in at least one scientific publication describing the effects of adding HCl to the pyrolysis gas.

SP Group:
SP Group has achieved theoretical expertise in calculation of pressure swing systems, and theoretical as well as practical know how in manufacturing of hollow fiber filter modules
The pressure swing module will only have relevance if the produced electricity is not competing with electricity produced by cheaper methods. This could be the case as a stand-alone system.

If hollow fibers are produced in large quantities it will be possible to produce fiber modules manufactured by casting the fibers into a leak tight sealing.

1.5 Project conclusion and perspective

FC and MEA optimizations
The project have been highly successful and paved the way forward for large HTPEM based CHP systems.
The initial concept of performance and durability optimization by operating the FC system at reduced temperatures and using oxygen enrichment of air, from surplus oxygen from an electrolyzer proved only feasible in a very narrow operating range. Optimized operating conditions were found, and a completely new phenomenon when operating with higher stoichiometries of oxygen and pressurised air was observed and explained.

Storage concept
The storage concept has potential, but has a higher cost than expected. As most of this is related to the storage tank we have discussed alternative storage concept using methanol or formic acid. The catalysts for the chemical conversion between these and H_2 + CO_2 are avail-

able but limited by the present catalyst efficiency and are is still in development. This concept would also necessitate the separation technologies investigated in this study which could therefore be relevant in a future project.

The project has demonstrated a safe way to store H_2, and designed a system that can use the stored H_2 during a period of 24 hours. The cost of the system is 2,4mill. dkr and the output is 88KWh/24h, if the mix is H_2/CO_2 = 40/60. However can the cost be reduced if the mix is changed to a higher consentration of H_2.

Separation
The Hollow fiber carbon membranes manufactured in this work have properties enabling them to separate H_2 and CO_2 and adding HCl to the pyrolysis gas is shown to increase the mechanical strength of the fibers. Even though the required membrane area is still quite large (hundreds of square meters for a 60 STP m^3/h feed stream), a reduction of the membrane thickness should increase the permeance, making the membranes more competitive.

Separation of other gas pairs with the manufactured membranes could prove of interest, since for instance the obtained CO_2/N_2 and O_2/N_2 selectivities were quite high for certain samples. Even though investigating this is beyond the scope of this project, it might become relevant at a later date.

1.6 Annual export of electricity (only ForskVE)

Not applicable

1.7 Updating Financial Appendix and submitting the final report

The financial appendix for the project period was submitted separately.

1.8 References

1. Robeson, L.M., *Correlation of separation factor versus permeability for polymeric membranes.* Journal of Membrane Science, 1991. **62**(2): p. 165-185.
2. Robeson, L.M., *The upper bound revisited.* Journal of Membrane Science, 2008. **320**(1–2): p. 390-400.

[1] F. Javier Pinar, P. Canizares, M. A. Rodrigo, D. Úbeda, J. Lobato, J. Power Sources 196 (2011) 4306–4313.
[2] F. J. Pinar, N. Pilinski, M. Rastedt, P. Wagner, Int. J. Hydrogen Energy40(2015) 5432-5438.
[3] Danish Power Systems - Homepage. 2015; http://www.daposy.com/.
[4] MKS Instruments - Homepage. 2015; http://www.mksinst.com/ index.aspx.
[5] Q. Li, J. O. Jensen, R. F. Savinell, N. J. Bjerrum , Progress in Polymer Science 34 (2009) 449–477.
[6] Y. Oono, T.Fukuda, A. Sounai, M. Hori, J. Power Sources 195 (2010) 1007-1014.
[7] S. Galbiati, A. Baricci, A. Casalegno, R. Marchesi, Int. J. Hydrogen Energy 38 (2013) 6469-6480
[8] Q. He, B. Shyam, M. Nishijima, D. Ramaker, S. Mukerjee, J. Phys. Chem. C 117 (2013) 4877–4887.
[9] R. Borup, J. Meyers, B. Pivovar, Y. S. Kim R. Mukundan, N. Garland,D. Myers, M. WILSON, F. Garzon, D. Wood et al., Chemical Reviews 107 (2007) 3904–3951.

[10] S. Søndergaard, L. N. Cleemann, J. O. Jensen , N. J. Bjerrum, to be submitted to J. Power Sources
[11] R. B. Getman, Y. Xu, W. F. Schneider, J. Phys. Chem. C 112 (2008) 9559-9572.
[12 H. Tang, A. Van der Ven, B. L. Trout Phys. Rev. B 70 (2004) 045420.